Visible, near-infrared spectrometry for simultaneous assessment of geophysical sediment properties (water and grain size) using the Spectral Derivative–Modified Gaussian Model.

Charles Verpoorter, V. Carrere, J-P Combe

AGU PUBLICATIONS

JGR

Journal of Geophysical Research: Earth Surface

RESEARCH ARTICLE
10.1002/2013JF002969

Key Points:
- We model geophysical properties of sediments using SD-MGM
- SD-MGM continuum is an indicator of water content and grain size
- Water types of natural sediment may be retrieved using the Gaussian analysis

Correspondence to:
C. Verpoorter,
Charles.Verpoorter@univ-littoral.fr

Citation:
Verpoorter, C., V. Carrère, and J.-P. Combe (2014), Visible, near-infrared spectrometry for simultaneous assessment of geophysical sediment properties (water and grain size) using the Spectral Derivative–Modified Gaussian Model, *J. Geophys. Res. Earth Surf.*, *119*, 2098–2122, doi:10.1002/2013JF002969.

Received 28 AUG 2013
Accepted 1 SEP 2014
Accepted article online 5 SEP 2014
Published online 2 OCT 2014

Visible, near-infrared spectrometry for simultaneous assessment of geophysical sediment properties (water and grain size) using the Spectral Derivative–Modified Gaussian Model

C. Verpoorter[1], V. Carrère[2], and J.-P. Combe[3]

[1]INSU-CNRS, UMR 8187, LOG, Laboratoire d'Océanologie et des Géosciences, Université du Littoral Côte d'Opale, Wimereux, France, [2]Laboratoire de Planétologie et Géodynamique, UMR CNRS 6112, Université de Nantes, Nantes, France, [3]The Bear Fight Center, Winthrop, Washington, USA

Abstract The main objective of this study is to extract from reflectance spectra the geophysical properties of mudflat sediments such as water content and grain size. As mentioned in the literature, difficulties remain in separating the respective contributions of grain size and water on the reflectance continuum. This paper deals with the evaluation of a new methodological approach, the Spectral Derivative–Modified Gaussian Model (SD-MGM) for establishing the relationship between the spectral features and the geophysical properties of sediments. The SD-MGM enables the deconvolution of spectra into two main components: (1) Gaussian curves for the absorption bands and (2) a straight line in the wave number domain for the portion of the spectrum that represents continuum. While the retrieved Gaussian features are known to be reliable indicators of the composition, it is shown that the retrieved continuum can be used as a novel approach for determining grain size and water content. Based on regression analyses between the SD-MGM spectral output parameters and the geophysical properties, a quantitative relationship between water content and the way in which the shape of the water band depth at 0.97 μm and 2.8 μm changes has been found during dehydration. It is shown that it is possible to separate three water types present in the sediment structure: saturated, free, and adsorbed waters with high coefficients of determination (r^2) of 0.97, 0.98, and 0.94, respectively. The continuum is also revealed to be a useful water content indicator because it is less affected by atmospheric effects.

1. Introduction

Among mudflat sediment properties, water content and grain size play a very important role across a range of sedimentary processes including biogeochemistry, sedimentation, sediment transport, erosion, and water exchange [*Le Hir et al*., 2000]. Accurate estimates of water content and sediment grain size are necessary for better understanding and modeling these processes. Conventionally, evaluation of these parameters is based on local point measurements. Remote sensing has become an important tool for mapping the spatiotemporal distribution of sediments [e.g., *Rainey et al*., 2000; *Smith et al*., 2004; *Deronde et al*., 2006] where other approaches generally require extrapolation of these point measurements. Since the early 1980s, in complement to the remote sensing observations, field and laboratory spectroscopy has been used to explore the relationship between reflectance spectra and selected physical and chemical properties of natural surfaces. Spectroscopy has proved to be useful to characterize both abiotic and biotic components such as minerals, organic components, photosynthetic pigments, water, and hydroxyl in clay lattices. It is well known that most biogeochemical components translate into absorption features at specific wavelengths and with specific shapes while the more physical properties (such as grain size, surface roughness, and illumination) influence the overall shape of the continuum [e.g., *Adams and Filice*, 1967; *Hunt and Salisbury*, 1970; *Hunt et al*., 1971a; *Hœpffner and Sathyendranath*, 1991; *Hapke*, 1993; *Clark*, 1999; *Carrère et al*., 2004; *Pommerol and Schmitt*, 2008b]. However, taking into account sediment properties all together remains complex and usually requires extensive fieldwork and laboratory investigations. This study focuses on water content and grain size estimates from reflectance spectra of mudflat sediments.

Moisture and grain size greatly influence the reflection of shortwave radiation from sediment surfaces in the visible near-infrared (VNIR, 0.4–1.1 μm) and shortwave infrared (SWIR, 1.1–2.5 μm) regions of the spectrum. Since the observations of *Ångström* [1925], the relationships between moisture content, grain size, and

reflectance has been studied by many authors [e.g., *Lobell and Asner*, 2002; *Whiting et al*., 2004; *Milliken and Mustard*, 2007a, 2007b; *Pommerol and Schmitt*, 2008a; *Small et al*., 2009]. However, deriving water content from mudflat sediment remains difficult, as the reflectance of sediment is not just a function of moisture but it also is affected by intrinsic factors such as, grain size, organic matter content, mineralogy, photosynthetic pigments from microphytobenthos when present, and also Sun-target-sensor geometry. *Small et al*. [2009] pointed out that moisture and grain size might be spectrally distinguishable. Therefore, additional experimental and modeling approaches are required to pursue this idea.

We have developed a new approach for simultaneous separation of grain size and water effects from reflectance spectra acquired during dehydration. The underlying objective was to provide complementary information about the spectral properties of sediments during the dehydration process of bulk sediment followed by testing of various grain sizes of natural sands. Similarly to the common absorption band analyses, we propose to use the reflectance continuum as an additional spectral indicator for predicting geophysical properties. Here we assume that grain size, surface roughness, water content, and organic matter influence the continuum in shape and intensity but at various degrees of magnitude. Several studies [*Milliken and Mustard*, 2005; *Pommerol and Schmitt*, 2008b] have already used the standard continuum removal technique [*Clark and Roush*, 1984] to estimate the continuum slope of mineral materials and predict water content. However, continuum removal was only applied to selected hydration absorptions at 1.9 μm and 3 μm. Although many hydration bands can be used under laboratory conditions for water prediction, some (1.4 and 1.9 μm, in particular) cannot be used in the field for terrestrial applications because they are partially masked by saturated atmospheric water vapor absorptions. Therefore, our laboratory investigation focuses on the 0.97 μm hydration band for estimating water content because it can also easily be used outdoors.

We present here a new approach relying on laboratory reflectance measurements acquired on mudflat sediments. We developed an algorithm allowing the estimation of both sediment water content and grain size using the strength of the 0.97 μm water absorption and the intercept of the continuum as derived from the Modified Gaussian Model (MGM) [*Sunshine et al*., 1990]. A Spectral Derivative (SD) analysis is performed to automatically estimate the starting parameters required for the MGM. This approach has the great advantage of deriving absorption features without a priori knowledge. In this paper, after providing a background on previous studies related to estimation of moisture content and grain size from spectral reflectance measurements of various soils and mudflat sediments, we describe the methodology followed to develop our new approach. We then provide a discussion on limitations and advantages of the proposed approach for the retrieval of geophysical properties. Finally, we propose a possible relationship that could allow for simultaneous estimate of both moisture content and grain size that needs to be tested further in various environments.

2. Background

2.1. Effects of Water Content on Overall Reflectance

Many studies have established the relationship between the amount of water in a soil and its reflectance. It is well accepted that the overall reflectance decreases with the increase of water content [*Bowers and Hanks*, 1965; *Dolgov and Vinogradova*, 1973; *Baumgardner et al*., 1986; *Twomey et al*., 1986; *Ishida et al*., 1991]. This effect was to some extent foreseen in 1925 by Ångström. Using a simple geometric model, *Ångström* [1925] proposed the concept of a total internal reflection mechanism within the film of water coating soil particles to explain the darkening effect by an increase of the probability of absorption by wet soil surfaces. *Dolgov and Vinogradova* [1973] considered a more complicated geometry including the water-air interfaces. Lower reflectance values with increasing water content was explained by the decrease of the relative refractive index of the medium surrounding the sediment particles as a result of water replacing air [*Twomey et al*., 1986]. For homogenous particles and since the refractive index of water is known, *Twomey et al*. [1986] proposed a model based on the idea of enhanced forward scattering. Most studies [*Bowers and Hanks*, 1965; *Bedidi et al*., 1992; *Lobbel and Asner*, 2002; *Whiting et al*., 2004; *Zhu et al*., 2010] revealed that the response of soils reflectance to the disappearance of water appeared to be nonlinear. *Small et al*. [2009] also demonstrated that the relationship between moisture content and reflectance is neither linear as was stated by *Idso et al*. [1975] for bare soils nor exponential [*Lobell and Asner*, 2002] but multiphase with a long linear dehydration stage followed by a rapid increase in reflectance and an asymptotic attenuation at the final stage of dehydration.

2.2. Effects of Water Content and Grain Size on Absorption Bands

In most studies published in the literature, regression techniques were used to predict grain size and/or water content properties from laboratory or in situ reflectance spectra. Several studies have already been conducted to determine an empirical relationship between dry to wet soil samples and absorption parameters of the hydration bands in the VNIR. The depth and shape of the water absorption bands were used to predict water content in a substrate [*Ben-Dor et al*., 1999; *Liu et al*., 2002; *Whiting et al*., 2004]. Using a predictive soil moisture model initially based on the degree of saturation and the reflectance value deriving from four sample sets, *Lobell and Asner* [2002] found that the SWIR region was more reliable to quantify water content than the VNIR region. Using partial least squares regression analysis between reflectance values deriving from eight wavelengths and water content based on three sample sets, *Zhu et al*. [2010] found that the absorption band at 1.89–1.99 μm provided the best prediction results. *Liu et al*. [2002] normalized the reflectance spectra of wet materials by their dry spectra. They found that based on seven selected wavelengths, normalized reflectance spectra were highly correlated to water content. *Lobell and Asner* [2002] observed that the metal-OH absorption band at 2.2 μm in soils was progressively masked when soil moisture content increased and attributed it to the broadening of the 2.8 μm fundamental liquid water absorption band.

Grain size influences the scattering-absorption relationship which is translated into the continuum and the spectral contrast of the absorptions. The nonlinear effect of grain size on reflectance spectra of pure or mixed minerals has been documented by many workers [*Adams and Filice*, 1967; *Pieters*, 1983; *Hapke*, 1993; *Gaffey et al*., 1993; *Mustard and Hays*, 1997; *Milliken and Mustard*, 2007a, 2007b]. Considering a homogenous composition, it has been demonstrated that a decrease in particle size results in an increase of both the number of scattering interfaces and the scattering volume. Indeed, as the mean optical path is shorter for fine grains than for coarse grains, scattering prevails on absorption and reciprocally. Scattering theory predicts that the spectral contrast of absorption bands depends on both mean path length and absorption coefficient [*Hapke*, 1993; *Shkuratov and Gruynko*, 2005]. Complex radiative transfer models enable the assessment of changes in particle sizes related to changes in reflectance if the absorption coefficients are known. However, the absorption coefficients for each component of sediments are generally unknown.

The effects of grain size and water content on reflectance have been studied extensively in laboratory and in field conditions, but fewer studies have paid attention to their combined effects. When varying both water content and grain size, the resulting spectral characteristics remain largely unknown. For wet particulate samples, *Peterson et al*. [1979] suggested that the range of albedo changes is related to particle size distribution of soils. *Small et al*. [2009] demonstrated that water content and grain size effects can be distinguished spectrally. Because grain size and water content controlled the shape of spectra and reflectance intensity in a relative and similar way, the retrieval of reliable quantitative information from reflectance spectra remains complex. Therefore, separating water and grain size information directly from spectral reflectance, particularly using spectral shape modeling, remains a challenge.

2.3. Absorption Band and Continuum Modeling

In spectroscopy, there is also an interest in the relationships between spectral features and the corresponding amount of absorbing materials. By definition [*Clark and Roush*, 1984; *Sunshine et al*., 1990], the continuum of reflectance is mainly influenced by photometric variations in relationship with scattering processes including albedo, viewing geometry, as well as absorption processes. To separate the water effect from the continuum of reflectance, absorption features can be isolated from the overall shape of the spectrum using the standard "continuum removal" technique [*Clark and Roush*, 1984]. Recently, *Rodger et al*. [2012] proposed a quadratic method in combination with continuum removal for estimating absorption features depth and location in the SWIR. Converting the reflectance into single-scattering albedo spectra and by removing the continuum, *Milliken and Mustard* [2005] found that hydration band analyses were more dependent on mineral composition than the mean optical path length or the normalized optical path length technique. *Whiting et al*. [2004] predicted the water content for numerous soils using the inverted Gaussian function (equation (1)):

$$R(\lambda) = R_{\lambda i} + (R_{\lambda 0} - R_{\lambda i}) \exp\left[\frac{-(\lambda_i - \mu_0)^2}{2\sigma^2}\right] \quad (1)$$

where $R_{\lambda i}$ is the maximum reflectance, $R_{\lambda 0}$ is the minimum reflectance, λ_i is the wavelength value at maximum reflectance, μ_0 is wavelength at 2.8 μm, and σ is the Gaussian function deviation parameter describing the

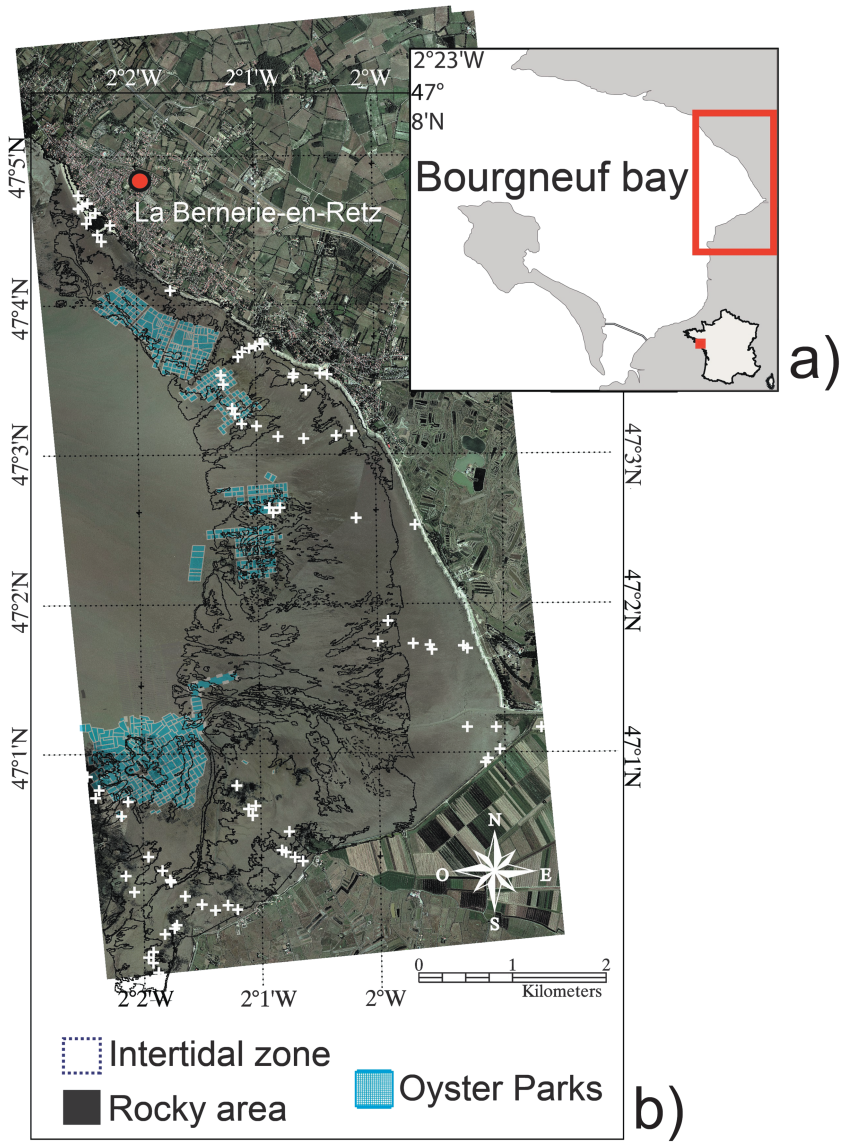

Figure 1. (a) Geographic position of Bourgneuf Bay (French Atlantic coast). (b) The orthophoto displays the studied site: it is the northeastern mudflat (red box). White crosses correspond to the sampled sites.

width of the Gaussian band. The index *i* indicates the band number varying from 1 to *n*. For each reflectance spectrum, the inverted Gaussian was used to extrapolate the spectral curve from the 1.2–2.5 μm range to the fundamental water absorption band which is theoretically centered at 2.8 μm. The shape of the inverted Gaussian function was attributed to the "continuum of water." In their analyses, the area shape parameter of the inverted Gaussian was found to be the best spectral predictor for water content assessments.

3. Study Area and Data Used

3.1. Study Area and Sampled Data

The tested area is located in the northern mudflat of Bourgneuf Bay, south of the Loire estuary (46–47°N, 1–2°W), on the French Atlantic coast (Figure 1a). The intertidal zone covers 100 km^2 of the total 340 km^2 of the bay area. Very few studies describing sedimentary facies of this area have been published [*Gouleau*, 1968, 1975]. They reported that the mudflat consisted mainly of cohesive fine mixed sediments (e.g., muddy and grain size $\leq$ 62.5 μm) but with an important fraction of noncohesive materials (e.g., sandy-sand and grains size $\geq$ 62.5 μm).

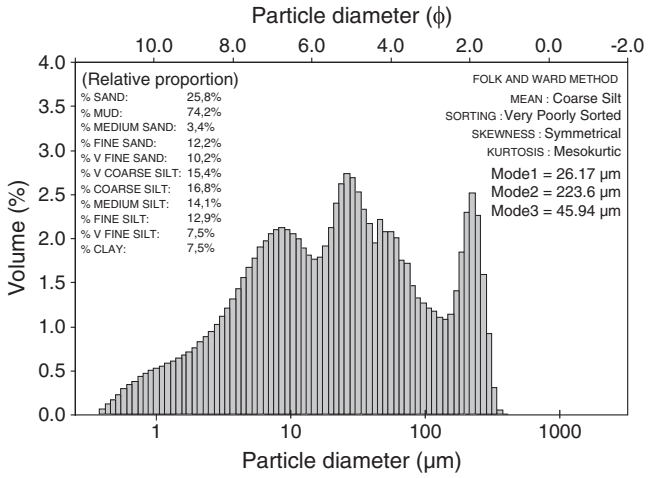

Figure 2. Histogram showing differential volume plots generated using the laser particle sizer Coulter^{TM} LS230 of a representative sediment sample (experiment 1) of the intertidal mudflat of the Bourgneuf Bay. The sample is polymodal and poorly sorted. The Folk and Ward method presents the advantages to retrieve the value of the secondary and tertiary modes and characterizes in the sample the relative percentages of sand, silt, and clay.

To determine which facies is the most representative of the mudflat, samples were collected during several field surveys. We systematically sampled ~200 g of sediment from the upper 2 cm of sediment and over an area of ~2 m^2 for each sampling site. A total of $n = 100$ samples were precisely located using a GPS device (Figures 1a and 1b, see white crosses). Sample compositions were analyzed to determine their mineralogy, organic matter, carbonate, and water content as well as grain size. X-ray diffraction (XRD) analyses were performed on selected nonconsolidated samples for assessing their mineralogical content [*Verpoorter*, 2009]. XRD analyses indicated that sediments were composed of quartz (78%), carbonates (18%), and feldspars (3%) associated with negligible amounts of mica, chlorite, amphibole, illite, smectite, and pyroxene. Clay mineral fractions were also found to be negligible, around ~ 1%. Organic matter content determined using the dry combustion method is low (~1–3%) with lowest values skewed to the right around 6–16% for 65 of the tested sites. Calcimetry investigations showed that ~15% of the 55 tested sites included carbonates. We selected only representative samples which better described the natural conditions in Bourgneuf Bay (quartz content = 78%; $CaCO_3$ content = 18.32%, and organic matter content = 0.90%) for our experiment.

Two techniques were used to determine grain size: (i) direct measurements from a laser diffraction particle size analyzer and (ii) dry sieving. The Coulter^{TM} LS230 laser was used to characterize natural well-mixed sediments. The selected sample was well mixed, and it varied from mud, muddy-sand, sandy-mud, to sand and was also poorly sorted (Figure 2). All these characteristics were consistent with previous studies [*Gouleau*, 1968]. This sample exhibited a trimodal distribution predominantly composed of not only clay (i.e., size fraction sensu stricto) and silt but also with an additional sandy component (Figure 2). Grain size distribution was used to calculate statistical parameters based on the grain size distribution and statistics (GRADISTAT) package [*Blott and Pye*, 2001]. These statistics included mean ($M_g = 22.63$ µm), median (D_{50} value: 22.75 µm), skewness ($S_{kg} = -0.049$), kurtosis ($K_g = 0.933$), sorting ($\sigma_g = 5.051$), and a measurement of the distribution spread defined by the difference between the percentile values ($D_{90} - D_{10} = 187.8$ µm). Additionally, we used Folk diagram to calculate the relative percentages of sediment fractions and describe the sedimentary texture. The textural group is sandy-mud; the relative proportions are 26% of sand and 74% of mud; thus, the sediment is called "fine sandy coarse silt."

3.2. Laboratory Surface Reflectance Measurements

An Analytical Spectral Device (ASD) Fieldspec3 FR® spectroradiometer was used to acquire sediment reflectance spectra in the wavelength range 0.350–2.500 µm and with a spectral resolution ranging from 3 nm (at 0.7 µm) to 10 nm (in the SWIR) resampled to 1 nm. Spectral sampling interval is about 1.4 nm from 0.35 to 1.0 µm and 2.0 nm from 1.0 to 2.5 µm. Spectral measurements were acquired using a high-intensity ASD contact probe allowing an elliptic nominal footprint sampling of about 12 mm × 10 mm [*Painter et al.*, 2007; *Zhu et al.*, 2010]. The optical contact probe configuration was used to be as much as possible close to the sediment surface; in that case, the optical configuration under which were measured reflectance spectra presents a constant and a nondirectional geometry. As described by *Painter et al.* [2007], the technique has lower uncertainty due to high signal-to-noise ratio and spectral resolution of the instrument and it avoids problems of variable illumination from surface topography and it accommodated slight changes in probe

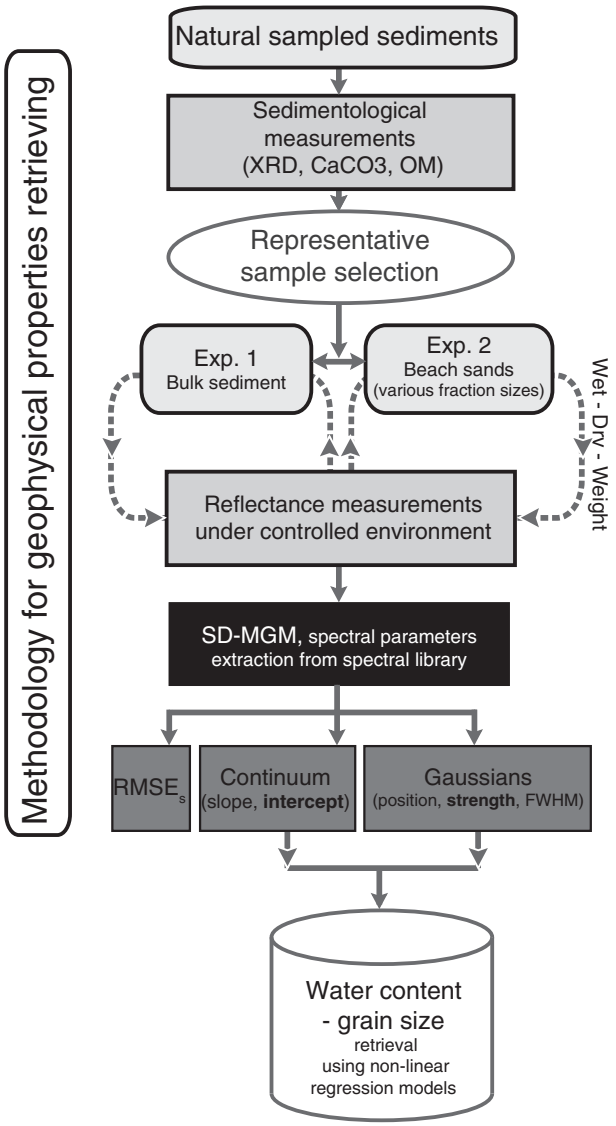

Figure 3. Flowchart representing the overall method used in this study.

orientation. Finally, a certified white Spectralon© panel $0.30 \times 0.30\ m^2$ (Labsphere, Inc.) was used to generate absolute-bidirectional reflectance spectra by dividing radiance spectra of the sediment samples by the radiance spectrum of the Spectralon.

4. Methodology

The overall methodology (see Figure 3) of this study can be summarized into two main steps. First, we assessed the spectral properties of sediments in a controlled environment. For this purpose, two sets of experiments were carried out: (1) on natural and poorly sorted sediments with varying water content (i.e., data set 1) and (2) with varying well-sorted sand fraction and water content for beach sediments (i.e., data set 2). While experiment 1 served to establish the relationships between water content, absorption bands and the continuum, understanding of the spectral behavior in response to dehydration also required knowledge of the grain size distribution for each measured sample. Therefore, experiment 2 was conducted with the objective to separate the different grain size fractions of sand sediments. This procedure is useful for discriminating water content from the grain size effects during dehydration and their impact on reflectance.

Second, statistical predictions based on the geophysical properties of sediments (i.e., data sets 1 and 2) and the spectral features deriving from the SD-MGM spectral curve fitting (i.e., Gaussians and continuum) were computed.

4.1. Relationships Between Water Content, Grain Size, and Reflectance

4.1.1. Experiment 1: Water Content Effects on Reflectance Properties

Concerning experiment 1 (Figure 3), sediment matter (~20 g) was put into individual petri dishes (diameter 5 cm) with a thickness of 2.0 cm, higher than the 1.5 cm that is considered to be optically thick [*Liu et al.*, 2002]. The sample surface was then lightly packed to obtain a flat and smooth surface at the millimeter scale. After measuring the reflectance of the oven-dried sample (150°C, for 24 h), de-ionized water was homogeneously distributed in the sediments using a syringe until they were completely saturated.

During the dehydration process, the samples were oven dried for a second time at 150°C until return of the sediment to its original mass. Because dehydration steps and relative weight loss are not continuous in time, reflectance spectra were acquired at nonconstant time intervals, based on relative weight loss. At each step, we weighed the sediment and measured its reflectance. An average of 20 individual spectra (Figure 4a) was used for each step, providing a noise level lower than 0.004 (Figure 4b), except at both ends of the spectral range which were not used in this study (i.e., below 0.4 μm and above 2.45 μm). The major sources of uncertainties for

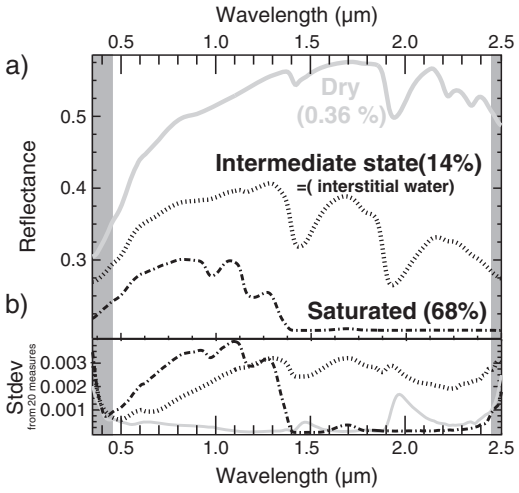

Figure 4. (a) Example of reflectance spectra of sediment (grey curve = dry state, dotted curve = intermediate state, and dash-dotted curve = wet state) acquired from an average of 20 measurements and (b) their associated standard deviation. The grey vertical bands represent the wavelength range where noise levels might be high.

all measurements presented in this study are associated with unwanted changes of sediment surfaces (roughness and density). To minimize the influence of the sediment surface roughness, reflectance spectra were acquired at each step after rotating the sample 4 times of approximately 90° counterclockwise. Little difference was observed between measurements (~2.4%). The Spectralon© panel was systematically measured before each sample measurement, using here again 20 scans. For each spectral measurement, the corresponding relative water content was concurrently measured by immediately weighing the samples. The mass loss of the different sample types after heating was measured in situ to determine the gravimetric water content (equation (2)) defined as

$$SMC(\%) = \frac{m_w\_m_d}{m_w} 100 \qquad (2)$$

where m_w was the weight of the wet sample and m_d was the weight of the dry sample. One of the sources of uncertainty for all measurements presented here is likely associated with permeability properties. The deeper layer was probably wetter than the surface due to high potential moisture retention by silt particles which concentrate at the bottom of the petri dish. The drying experiments were stopped as soon as the recorded spectra did not exhibit sustainable significant changes and until the water mass level was stabilized. Because in natural condition mudflat sediments are poorly sorted, we developed an additional experiment to derive simultaneously grain size and water content from reflectance spectra for well-sorted siliceous sediments.

4.1.2. Experiment 2: Grain Size Effects on Reflectance Properties

Experiment 2 was designed to understand the relationships between grain size fractions and spectral reflectance changes (i.e., absorption and continuum parameters) during dehydration (Figure 3). For each of the obtained size fractions, the dehydration protocol was rigorously performed in the same way as the one described just before. We restricted experiment 2 to a basic sand composition mainly dominated by siliceous materials without organic matter or other minerals. Organic and carbonate components were removed using hydrogen peroxide and acid attack, respectively. Because quartz can have weak or nonexistent absorption in the VNIR [*Clark*, 1999], the use of such a basic composition is relevant to isolate the spectral contributions of water and grain size. Grain size fractions were separated out into nine size classes by dry sieving. We used a sieve column containing the following sieves: <35, 35–50, 50–71, 71–100, 100–141, 141–200, 200–280, 280–400, and 400–800 μm. Spectral measurements were performed for each grain size fraction, and the derived observations are assessed in detail in section 5.

4.2. Spectral Curve Fitting

Our study investigates the potential of the Spectral Derivative–Modified Gaussian Model (SD-MGM) method [*Verpoorter et al*., 2007] to extract geophysical properties which enables the modeling of the overall shape of the spectra taking into account both the specific absorption band of liquid water at 0.97 μm and the reflectance continuum.

4.2.1. Background on the MGM

Our work consisted in separating grain size from water spectral effects and performed quantitative spectral modeling of sediments using VNIR reflectance spectroscopy. As hydration absorption bands were superimposed to the continuum, we propose to deconvolve reflectance using the SD-MGM. SD-MGM is an improvement of the original Modified Gaussian Model (MGM) initially developed by *Sunshine et al*. [1990] and adapted for large data set processing by *Combe et al*. [2005]. The MGM is able to deconvolve successfully overlapping absorptions [e.g., *Sunshine and Pieters*, 1993; *Mustard et al*., 1997; *Noble et al*., 2006]. However, different initial parameters could result in nonunique solutions, and the final band parameters are influenced by

the starting band positions [*Kanner et al*., 2007]. Spectral derivative (SD) analyses were used to stabilize the MGM inversion process by providing an appropriate a priori knowledge [*Verpoorter et al*., 2007]. The advantage of the MGM is that it provides a good estimate of the overall shape or continuum which cannot be explained by the absorptions. The continuum shape is described as a polynomial form in the wavelength domain and fits along with the Gaussians (see *Sunshine et al*. [1990] for details). The natural logarithm of a reflectance spectrum can thus be modeled (Figure 6c, blue curves) as a sum of n absorption bands superimposed on a MGM continuum. The MGM provides a model for the continuum as an empirical mathematical function (see *Sunshine et al*. [1990] for details). Since no physical model for continua is provided by the scattering theory in a solid system, we selected a linear function of wave numbers (inverse of wavelengths), which best fits the shape of our measured spectra. An intercept and a negative slope provide the best approximation for the continuum we observed. Both are supposed to be constant parameters inherent to the host constituent (sediments). Although MGM computations are carried out in wave number and natural log reflectance, for convenience, most of figures are displayed in reflectance as a function of wavelength.

4.2.2. MGM Starting Parameters and Inversion Process

MGM is a semi-automatic process that relies on the stochastic inversion and partial least squares analysis of *Tarantola and Valette* [1982] that uses partial derivatives. The inversion process is described in details by *Sunshine et al*. [1990]. It needs an initial set of parameters representing a priori information as constraints on the solutions. *Sunshine and Pieters* [1993] demonstrated that constraints are necessary to prevent physically unrealistic solutions and stabilize the inversion process. Spectral fitting is constrained by the model for the absorption bands and the continuum. Each absorption band is modeled by three parameters: position, full width at half maximum (FWHM proportional to the standard deviation, σ), and strength. Each parameter is defined by a central value and an interval of uncertainty that constraints the magnitude of change during the inversion. The inversion of a spectrum adjusts simultaneously all the model parameters (Gaussian widths, strengths, and centers, as well as continuum slope and intercept) by an iterative process. The set of MGM parameters is solved iteratively using first-order Taylor expansion of the MGM equation. Finally, the iterative process described by *Tarantola and Valette* [1982] converges to a solution that is acceptable if the residual becomes lower than a defined threshold ($\mathrm{RMS}_{\max} = 1 \times 10^{-4}$). The residual error (Figure 6c, orange curve) corresponds to the difference between the measured natural logarithm reflectance spectrum $R(\lambda)$ and the modeled spectrum $R'(\lambda)$. The quality of the modeled spectrum is described by the root-mean-square of the residual error, RMSE_s (equation (3)):

$$\mathrm{RMSE}_s = \sqrt{\sum_{i=1}^{n} \frac{\left(R(\lambda_i) - R'(\lambda_i)\right)^2}{n}} \tag{3}$$

where λ is the wavelength, n the number of channels, and i an index varying from 1 to n. An average of the RMSE_s is commonly used to sum up the quality of the spectral modeling during dehydration process. Additionally, standard deviation values (SD_s) from the SD-MGM fit are also given.

In the original version, the choice of the starting MGM parameters is left to the user and thus requires some initial knowledge on surface composition. When this knowledge does not exist or when surface composition varies too much, an automatic evaluation of the initial set of parameters becomes more appropriate. As demonstrated by *Kanner et al*. [2007], the final band parameters are highly correlated to the initial band parameters. In order to avoid such problems, we used spectral derivative analysis to derive a set of starting parameters for the MGM without a priori knowledge.

4.2.3. Background on Spectral Derivative Analysis

Derivative spectra indicate the rate of change in reflectance as a function of wavelength ($\mathrm{d}\rho(\lambda)/\mathrm{d}\lambda$), which is the slope of the reflectance curve at wavelength λ [*Dixit and Ram*, 1985; *Talsky*, 1994]. We have explored the properties of spectral derivative analysis in order to automatically extract absorption features from reflectance spectra. For instance, our procedure was already successfully implemented for determining composition of Mars surfaces from hyperspectral images [*Massé et al*., 2010, 2011]. Here the purpose is to account for the spectral diversity of measurements and to help with the MGM parameterization by determining the number of absorption bands in a spectrum and the characteristics of the modified Gaussian curves. In the initial MGM estimate, derivative analysis solves the number of Gaussians to be used, their central wavelength position, and their shape (strength, FWHM). Taking the advantage that derivative analysis has been proven to differentiate overlapping signatures and resolve weak features [*Huguenin and Jones*, 1986] and that derivation of reflectance

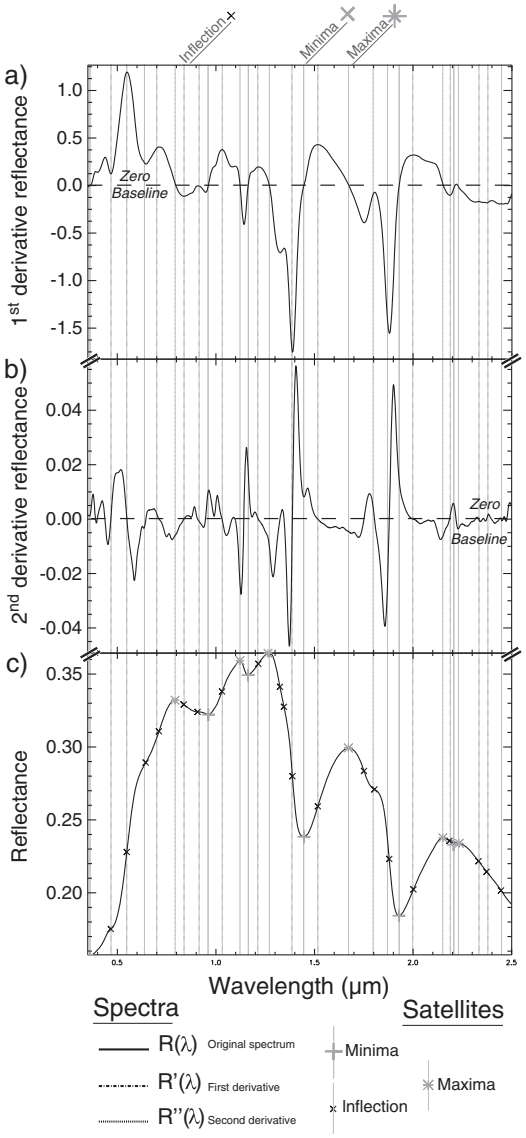

Figure 5. Spectral Derivative Analysis on hydrated sediment spectrum ($H_2O = 9\%$). (a) First derivative order and (b) second derivative order. (c) Original spectrum, satellite points are represented by vertical lines, and crosses represent local minima. Vertical dashed lines and stars represent local maxima, and vertical dotted lines and diamonds represent inflection points.

spectra is insensitive to the background signal [*Philpot*, 1991; *Tsai and Philpot*, 1998; *Demetriades-Shah et al*., 1990], we applied this simple technique for inverting the absorption parameters of MGM independently from background signal. According to *Huguenin and Jones* [1986], continuum contributions, phase angle effects, and broad low-frequency calibration errors are minimized. Derivatives of second order or higher should be relatively insensitive to variations in illumination intensity, Sun angle, and small topographic effects. This is explained by the fact that derivation also places all absorption features on the same reference plane (i.e., centered on zero in the first derivative). For example, in water color applications, *Goodin et al*. [1993] suggested that the first- and second-order derivative transformations reduce interference from the background on the derivative spectra observable in the VNIR region and also reduce the effect on the general shape of the spectra. Consequently, no continuum removal is needed prior to modeling Gaussian bands [*Huguenin and Jones*, 1986].

4.2.4. Methodological Development: Step by Step Procedure of the SD-MGM

The SD-MGM procedure included the following steps:

1. Data smoothing [*Savitzky and Golay*, 1964], as the band detection performed by derivative analysis is known to be sensitive to noise. Because our measurements exhibit a high signal-to-noise ratio, the impact of noise on our procedure is minimum.
2. Spectral Derivative analysis, in order to identify spectral absorptions features and to build a set of initial absorption parameters for the MGM. Derivatives are calculated for the center point of the sliding segment using the coefficients of the second-order derivative. Higher-order derivatives are substantially noisier and therefore require high signal-to-noise ratio to be useful. Although our data were rather "clean," we restricted our analyses to first- and second- order derivatives for a more general evaluation of our approach.

The inflection points in close bands become turning points in the first derivatives (Figure 5a). The first-order derivative shows that all representative spectral bands selected above the zero baseline coincide with inflections of the curves. Peaks in the first derivative reveal the rate of change in slope of the original spectrum. Zero values in first derivatives pinpoint accurately the minima positions of broad absorptions or peaks. The sign of "'zero crossing" indicates local maxima (negative sign) or local minima (positive sign) in the original spectrum (Figure 5c). The second derivative (Figure 5b) gives us access to asymmetry (high magnitude), minima and maxima (derivative sign), and spectrum slope (when equal to zero). Consequently, the position of absorption bands can be accurately determined by the use of the first and second derivative

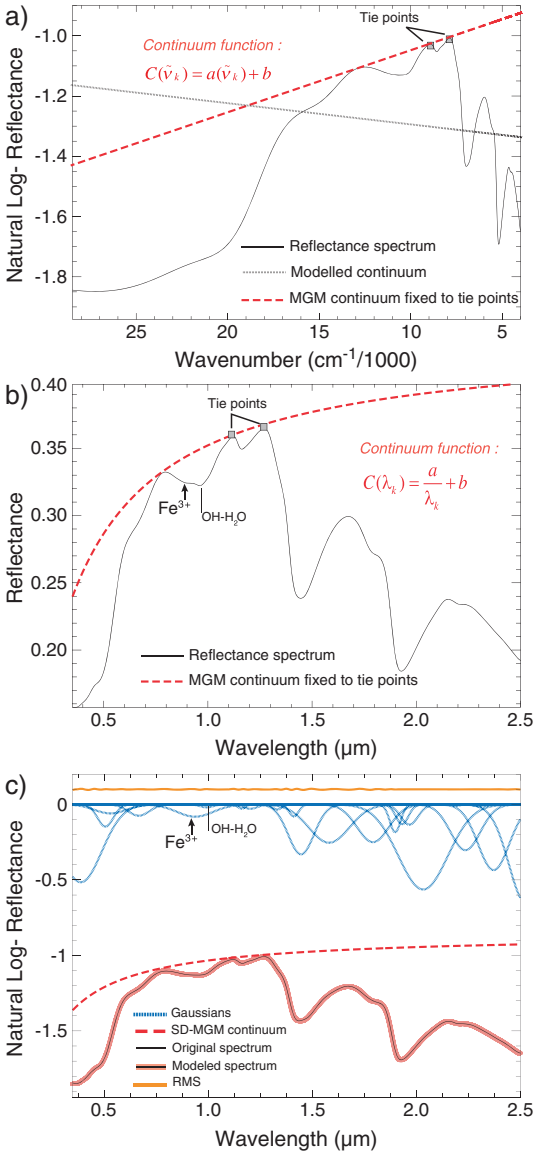

Figure 6. (a) Example of visible and near-infrared spectrum (reflectance curve displayed in wave number and natural log reflectance) of hydrated sediment ($H_2O = 9\%$, with a range of grains size of 400–800 µm) and the MGM modeled continuum (dotted curves initially modeled in natural logarithm domain). The MGM continuum (red dashed curves) is transposed to the tie points (i.e., local maxima of the spectra). (b) The same spectrum but in the reflectance domain and (c) displayed in natural logarithm domain after SD-MGM deconvolution process. Note that electronic transition process which is translated into broad ferric absorption feature adequately overlaps the hydration band at 0.97 µm.

orders. Spectral derivative analysis is also capable of individualizing absorption bands even when overlaps hide local minima in reflectance spectra (Figure 5c). In SD-MGM, the number of Gaussians is determined by a combination of local minima and a subset of inflection points. Band position retrieval was described above. As for as the amplitude of the initial Gaussian band is concerned, it corresponds, in first derivative spectra, to the distance between the maximum peak and the minimum peak, also called magnitude. Knowing the amplitude of the Gaussian, FWHM is approximated using two consecutive local minima in the second spectral derivative.

1. The initial set of parameters is simply completed with an estimate of the continuum parameters (slope and intercept). Following the *Sunshine et al.* [1990] mathematical representation of the continuum, it was automatically modeled following its linear form in discrete energies (wave number domain) and in natural logarithm reflectance (Figure 6a) to be turned into its polynomial form in the wavelength domain (Figure 6b). Here the continuum was fitted to the spectrum shape using a least absolute deviation method and transposed at the stable local maximum of reflectance. Our initial guess for the starting slope and intercept use contact points at local maxima of the spectrum also detected by derivative analysis. This simple continuum approximation is an acceptable initial solution, because it allows the convergence of the iterative process. Then, after parameterization, the continuum was fitted simultaneously with Gaussians (Figure 6c).
2. Running the MGM using the spectral derivative optimization as input (SD-MGM). As mentioned in previous section, all the output parameters described above were iteratively adjusted during MGM process using the partial least squares approach. Output spectral parameters contain information about abundance of materials and physical parameters of the sediments.

Among the model output parameters, we will mainly focus on the modified Gaussian absorption strength (called for simplification, Gaussian strength (GS)) of the 0.97 µm hydration band and parameters describing the continuum. In case of overlapping bands within the [0.835–1.035 µm] wavelength range, we selected the Gaussian which was closer to the 0.97 µm hydration band.

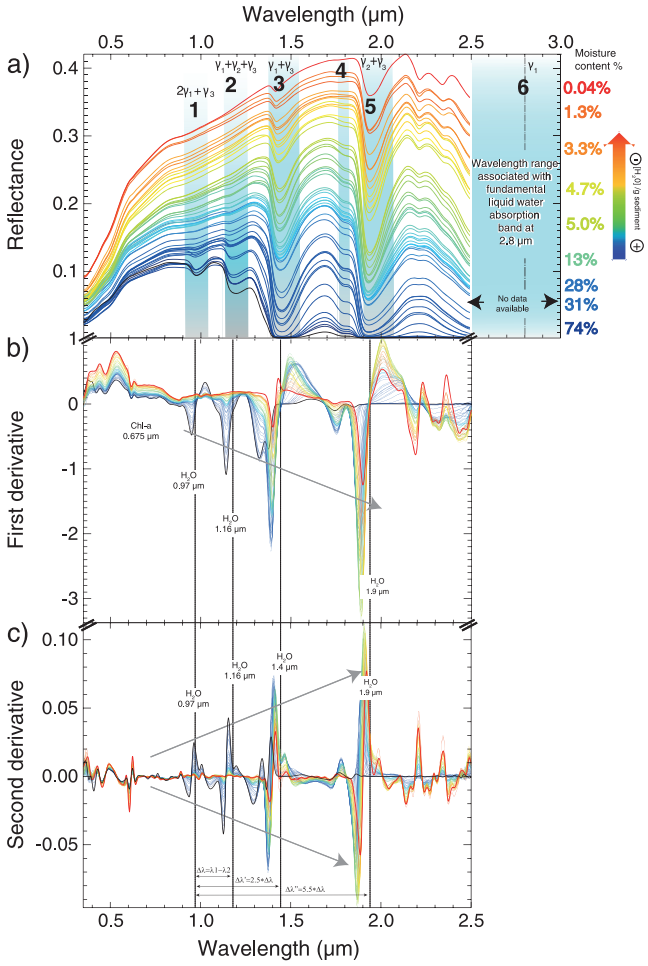

Figure 7. (a) Sandy-mud spectral reflectance measured during dehydration (blue to red) between 0.35 and 2.5 μm with an ASD (Fieldspec3 pro FR) spectroradiometer (experiment 1). Effects of moisture variation on reflectance spectra, major absorption region for sandy-mud sediment and bands with numbers 1–6 are assigned to combinations between fundamental and overtones vibrations in water stretching and bending (γ_1 symmetric stretching at 2.73 μm, γ_2 bending mode at 6.27 μm, and γ_3 asymmetric stretching at 2.66 μm), and their comparative energy absorption strengths. (b) Changes in first derivatives of reflectance and plots $d\rho(\lambda)/d\lambda$. (c) Changes in second derivatives. Spectra derived from sediment with high moisture content show high-magnitude peaks; arrows indicate the increasing magnitude of peaks.

4.3. Regression Analyses

To represent the relationships between the water content and the spectral properties, some researchers have used linear regression models [*Rainey et al.*, 2003; *Whiting et al.*, 2004], polynomial [*Adam et al.*, 2011] with or without logarithmic or derivation transformations [*Yen et al.*, 1998; *Suehara et al.*, 1999; *Zhu et al.*, 2010], while others have used multiple regression analyses [*Faraji et al.*, 2004]. Since it is well established that water content and grain size have a nonlinear effect on reflectance [*Lobell and Asner*, 2002; *Milliken and Mustard*, 2007a, 2007b], an exponential decay regression law was used here to model the relationships between SD-MGM parameters (GS, continuum intercept) and the mean grain size and water content. It is also convenient to use an exponential function such as the Beer Lambert law to determine the relationships between absorption depths and abundance.

An aliquot of each sample is used as a calibration set from which the regression laws are derived and as a validation set. The quality of the calibration models is evaluated by computing statistical parameters: correlation coefficient of the calibration data set r^2_c, root-mean-square error for $RMSE_c$ (equal to the square root of reduced χ^2), the associated standard error (SE), standard deviation (SD), and probability p level. Finally, once the calibration models are generated, they are confirmed using a separated validation set. Similarly to the calibration data, correlation coefficient of the validated data set r^2_v and root-mean-square error for validation set $RMSE_v$ were calculated.

5. Results

5.1. Water Content

5.1.1. Spectral Reflectance Response to Water Content Variations

Figure 7a shows the water-induced strong variability in sediment reflectance on both the overall shape of the spectrum (i.e., continuum) and the specific hydration bands during dehydration. The plot displays the reflectance measurements of the natural sediment (i.e., data set 1). In the [0.4–3.0 μm] spectral range, water induces the occurrence of five overtones at 0.97, 1.20, 1.40, 1.79, 1.90 μm, and one fundamental absorption band at 2.8 μm [*Collins*, 1937; *Whiting et al.*, 2004]. Note that the fundamental water absorption band at 2.8 μm

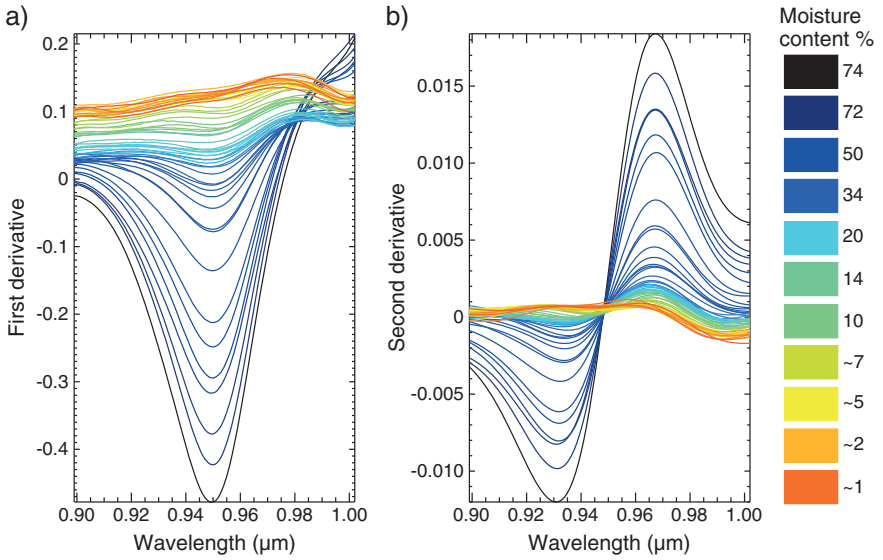

Figure 8. Absorption sensitivity at 0.97 μm in response to dehydration is revealed by changes in derivatives of sandy-mud reflectance spectra (blue to red). Spectra were collected between 0.90 and 1.0 μm using the same scale color as Figure 7. Changes in (a) first and (b) second derivatives reflectance ($d\rho(\lambda)/d\lambda$) display significant magnitudes even for small water content. Magnitude changes below ~3.5% of water content appeared less significant and uncertain.

is out of the ASD spectral range [0.35–2.5 μm]. In our context, it was observed that when the water form changed, it appeared systematically as a critical change in the reflectance properties. Saturated water was defined when water covered most particle surfaces and filled the macropores and micropores of the sediment structure. Free water was defined as capillary water or bulk water filling macropores and micropores. Water released by heating from sediment samples initially originated from macropores, micropores, and finally from the surface of grains (i.e., adsorbed water), interlayered in clays, bound in the mineral phase as H_2O, or hydroxyl (OH) within the structure. For instance, an abrupt shift in the reflectance values was systematically observed in the final stage of drying, particularly in the infrared part of the spectrum. When free water is removed from the pores of the sediment structure, some water remains adsorbed on the particle surfaces; this phenomenon is translated into a drastic change of reflectance. Note that this abrupt increase in the reflectance measurements is in agreement with the *Lobell and Asner* [2002] and *Small et al.* [2009] observations.

Spectral variations on the absorption bands were highlighted by the use of spectral derivatives ($d\rho(\lambda)/d\lambda$) of the reflectance values [*Huguenin and Jones*, 1986; *Talsky*, 1994; *Tsai and Philpot*, 1998]. Figures 7b and 7c exhibit peak variations which are related to the absorption band changes. The magnitudes of the peaks decrease with the decrease in water content (the ratio between band depth and band width decreases). Conversely, at a given water content, the magnitude of the peak increases with wavelength (the overtone absorption bands that are closer to the fundamental mode wavelength are more pronounced). For the hydration band at 0.97 μm (Figures 8a and 8b), significant variations in first and second derivative values were always observed meaning that the absorption band is sensitive to wide range of water contents. However, although derivative values changed monotonically with dehydration, no clear trend can be observed for water contents lower than ~3.5%, meaning that the water content prediction at 0.97 μm might be less accurate in this range.

5.1.2. Absorption at 0.97 μm

Spectra of experiment 1 for various water contents are modeled by the SD-MGM iterative process, with a low average $RMSE_s$ (0.0029) and SD (0.0018). Then, for the calibration set ($n = 52$), the $GS_{0.97\ \mu m}$ is regressed against the gravimetric water content (Figure 9a). It is observed that the Gaussian strength increases with water content, which is consistent with the absorption theory (see section 2.2). However, the relationship between absorption strength and water content exhibits three different sections which can be identified from the regression curves. We assume that these spectral responses are probably correlated to the different hydration states of sediment such as saturated water, free water, and adsorbed water.

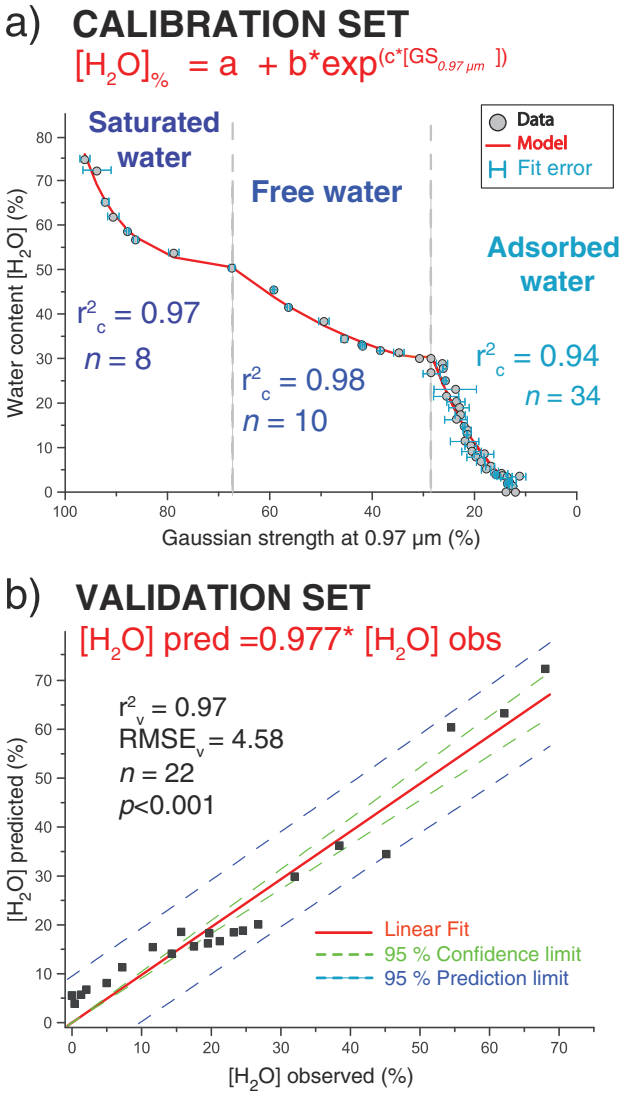

Figure 9. (a) Exponential models for estimating water content after SD-MGM procedure. *X* axis is the measured water content in the sample; *Y* axis is the estimation of the strength of the specific liquid water absorption at 0.97 µm for a sandy-mud sediment sample. The correlation coefficient is r^2. The number of observations is *n*. The significance is *p*. It is possible to separate three presumed water forms: (1) saturated water, (2) free water, and (3) adsorbed water. (b) Comparison between water content measured in the sample and predicted water content derived from the depth of the 0.97 µm absorption band.

Model accuracy is considered to be acceptable when fit error associated with the $RMSE_s$ is contained within the prediction limits of the three models (see blue bars in Figure 9a). Correlation coefficients (r^2) calculated for each hydration form are good, 0.98, 0.97, and 0.94, respectively. Table 1 summarizes product moment coefficients calculated from the correlation between water content and specific liquid water absorption band, and regression model equations. Goodness of fit is expressed as a low average $RMSE_c$ (1.307%).

Validation performed on the test data set ($n = 22$) also gives a high r^2 of 0.97 with a slope of ~0.977 close to the 1:1 line (Figure 9b). The resulting underestimation (2.3%) may be considered to be negligible. Variance from the repeated Gaussian strength measurements is used to compute the confidence limits (green dashed line), while standard deviation is used to calculate the prediction limit (blue dashed line). Note that the water content prediction using the spectral models is within these limits. The exponential models are validated and can be applied in laboratory conditions for water content predictions. For water content lower than 3.5%, uncertainties associated within the prediction limits increase due to the fact that the SD-MGM is less accurate in that range and because the 0.97 µm water band is not sensitive enough for such low values.

5.1.3. Intercept of the Continuum

We also investigated the possibility to use the continuum as a proxy for water content estimate. We developed a simple exponential model based on empirical relationships between water content and the intercept of the continuum as derived by SD-MGM (Figure 10a).

Following our experimental observations, the overall reflectance decreases with the increase of water content, which is consistent with the absorption theory (see background section 2.2). Note that no significant relationship between water content and continuum slope could be found, probably due to the fact that the combination of the individual and overlapping Gaussians compensates the slope variation of the continuum. During dehydration, albedo variations are mainly translated into the intercept parameter of the SD-MGM's continuum. The resulting model is summarized in Table 2.

In Figure 10a, a strong correlation between water content and the continuum intercept is observed for the calibration set ($r^2_c = 0.96$). The goodness of fit and error statistics for the validation set are as follows: $r^2_v = 0.98$

Table 1. Calibration and Validation Models of SD-MGM Hydration Absorption Bands[a]

Calibration Set

Water forms	*a* (SE)	*b* (SE)	*c* (SE)	*n*	r_c^2	$RMSE_c$
Saturated	49.81 (1.7754)**	42.02 (4.0463)--	−0.125 (0.0219)***	8	0.97	1.2757
Free	19.98 (4.3357)***	88.57 (12.602)-	−0.032 (0.0007)**	10	0.98	0.7770
Adsorbed	−12.23 (5.8238)***	8071 (9906.3)***	−0.073 (0.0183)***	34	0.94	1.8662

Validation Set

Water forms	*a* (SE)	*b* (SE)	*n*	r_v^2	$RMSE_v$
ND	0.977 (0.033)***	-	22	0.97	4.58

[a]ND stands for nondefined and NS for nonsignificant. Student *t* test probability: −−: NS. *: $\rho < 0.05$. **: $\rho < 0.01$. ***: $\rho < 0.001$. Product moments are the correlation coefficients: (r^2), number of measurements (*n*), and root-mean-square error (RMSE). Equations coefficients *a*, *b*, or *c* are given with their standard error (SE).

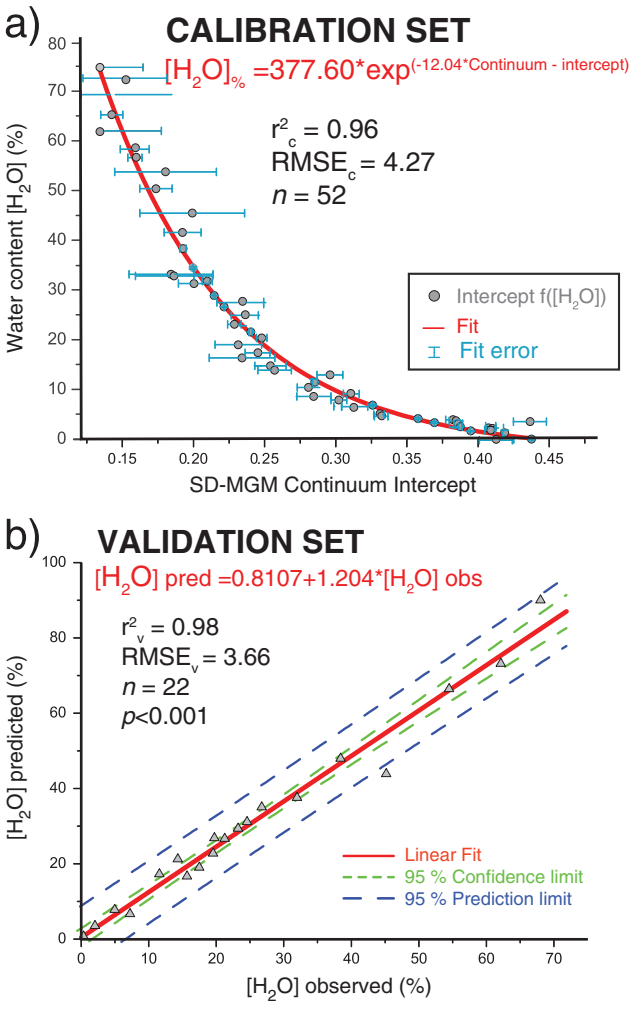

Figure 10. (a) Exponential model for estimating water content after SD-MGM procedure. *X* axis is the estimation of the continuum intercept for a sand sediment sample. *Y* axis is the measured water content in the sample. Coefficient of correlation (r^2), number of observations (*n*), and probability (*p*) are also given. (b) Comparison between water content measured in the sample and predicted water content derived from the continuum intercept.

and $RMSE_v = 3.66$. Despite the well-defined linear regression, the slope ($a = 1.2$) deviates from the 1:1 line (Figure 10b) with an overestimation of ~20%. These preliminary results regarding the continuum suggest that the approach developed here might be considered for water content assessment, but it is less accurate than the hydration band prediction.

5.2. Grain Size

5.2.1. Spectral Reflectance Response to Grain Size Variations

Figure 11a shows reflectance spectra from experiment 2 for each of the dry sand fractions. Note that the spectra of sand systematically display a relative broad absorption band in the SWIR at 2.2 μm due to Si-OH vibrations and which are attributed to the fraction of amorphous silicate minerals [*Hunt and Salisbury*, 1970]. Additionally, a broad absorption band in the visible range attributed to iron oxide was observed (see red spectrum of Figures 11a and 11b). Iron oxide is spectrally active across the VNIR spectral range via charge transfer processes, which are responsible for the broad iron absorption band [*Hunt et al.*, 1971a]. A visual inspection was performed using a scanning electron microscope. A thin reddish deposit of hematite coating quartz particles was observed; this phenomenon is also called rubification of quartz [*Ben-Dor et al.*, 2006]. Fortunately, hematite coating was mainly present at the surface of the

Table 2. Calibration and Validation Models of SD-MGM Intercept Continuum[a]

Calibration Set

Water forms	*a* (SE)	*b* (SE)	*c* (SE)	*n*	r_c^2	$RMSE_c$
ND	-	377.60 (33.226)***	−12.04 (0.4947)***	52	0.96	4.27

Validation Set

Water forms	*a* (SE)	*b* (SE)	*n*	r_v^2	$RMSE_v$
ND	1.204 (0.042)***	0.810 (1.278)--	22	0.98	43.66

[a]ND stands for nondefined and NS for nonsignificant. Student *t* test probability: −−: NS. *: $\rho < 0.05$. **: $\rho < 0.01$. ***: $\rho < 0.001$. Product moments are the correlation coefficients: (r^2), number of measurements (*n*), root-mean-square error (RMSE). Equations coefficients *a*, *b*, or *c* are given with their standard error (SE).

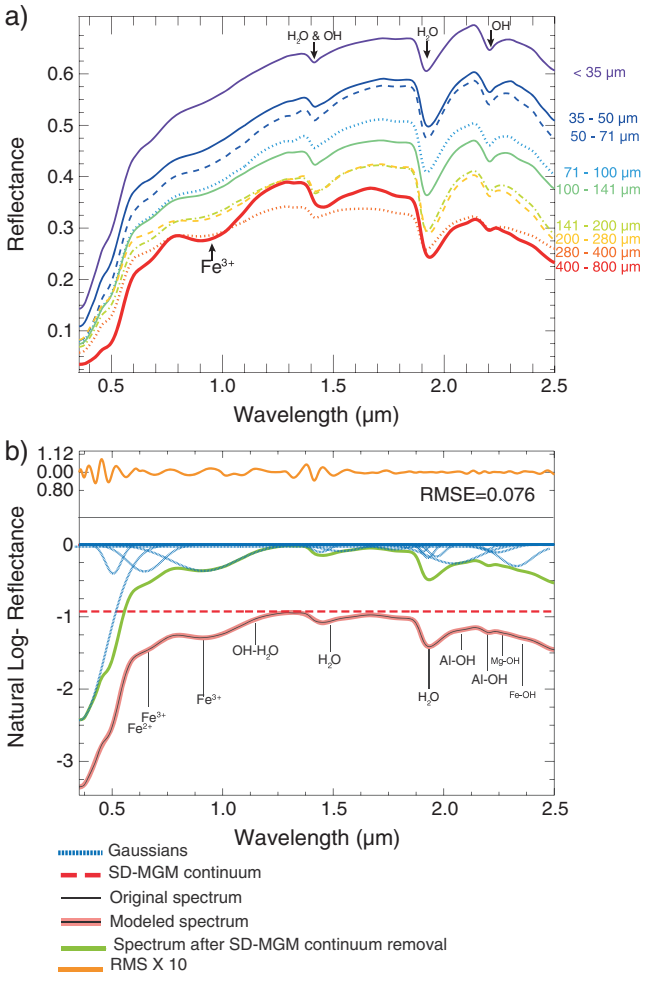

Figure 11. (a) Spectral reflectance of dry beach sands measured between 0.35 and 2.5 µm with an ASD (Fieldspec3 pro FR) spectroradiometer (experiment 2). Effects of grain size increase (blue to red) on dry reflectance spectra. For the coarsest class (red spectrum), broad absorption in the VNIR is attributed to iron oxide effect, and (b) SD-MGM spectral deconvolution corresponding to the same spectrum at 400–800 µm. Reflectance values are transformed in the natural logarithm reflectance domain. Note that for this case the shape of the continuum is linear in the wavelength domain instead to be polynomial due to the ferric broad absorption features.

coarser grains [400–800 µm]. Because dry siliceous materials generally do not present any spectral features in the VNIR, we can assume that a change in grain size should only induce a change in the overall shape of the spectrum or continuum behavior. Furthermore, the dehydration affects both the shape of the continuum and specific hydration bands.

5.2.2. Intercept of the Continuum

As mentioned above, the continuum is also influenced by grain size variations; hence, it is interesting to investigate if the SD-MGM can also be used for retrieving a reliable relationship between grain size and continuum parameters.

Concerning experiment 2, for each of the nine mean-size fractions, it is shown that the calculated average $RMSE_s$ is very low, indicating a good match between original and modeled spectra (Table 3).

We observed that the intercept values of the continuum exponentially increased as a function of moisture content for all size fractions (Figure 12a). Again, these results confirm that the SD-MGM continuum can be used as a good indicator for predicting water content when grain size is known. Plot lines exhibit different degrees in their curvature, ranging from a low concavity for fine particles to a strong concavity for coarse particles. When comparing all of them for a given water content, a clear differentiation appears between grain size and water content effects on the continuum. A clear pattern can be identified (see arrow Figure 12a),

Table 3. Calibration Models of SD-MGM Intercept Continuum[a]

SD-MGM			Calibration Set				
Grain size	$RMSE_s$	SD_s	*a* (SE)	*b* (SE)	*n*	r_c^2	$RMSE_c$
35 µm	2.960×10^{-3}	1.455×10^{-3}	234.07 (33.2260)***	−6.2405 (0.4947)***	27	0.93	6.1755
45 µm	3.819×10^{-3}	2.139×10^{-3}	274.07 (38.6517)***	−6.9864 (0.4675)***	27	0.91	4.5011
60 µm	3.321×10^{-3}	1.613×10^{-3}	369.47 (34.6753)***	−8.2980 (0.3834)***	26	0.96	3.8119
85 µm	2.947×10^{-3}	1.558×10^{-3}	230.09 (41.4429)***	−6.8802 (0.7927)***	18	0.88	8.3498
120 µm	3.270×10^{-3}	1.843×10^{-3}	190.84 (22.5279)***	−8.1420 (0.6331)***	22	0.93	4.1931
170 µm	4.326×10^{-3}	1.183×10^{-3}	277.95 (39.3178)**	−10.876 (0.7591)***	28	0.92	4.6702
240 µm	5.820×10^{-3}	1.538×10^{-3}	459.56 (131.335)***	−14.302 (1.613)***	22	0.78	6.8641
340 µm	4.742×10^{-3}	1.860×10^{-3}	375.75 (121.330)*	−15.023 (2.300)***	25	0.75	8.5715
600 µm	5.467×10^{-3}	1.694×10^{-3}	781.84 (247.191)*	−17.436 (2.065)***	31	0.76	6.7771

[a]Student *t* test probability: −−: NS. *: $\rho < 0.05$. **: $\rho < 0.01$. ***: $\rho < 0.001$. After SD-MGM deconvolution, the average of the root-mean-square error ($RMSE_s$) and standard deviation (SD_s). The exponential equation coefficients such as *a* and *b* are associated with their standard error (SE), correlation coefficients of calibration set (r^2_c), number of measurements (*n*), and root-mean-square error ($RMSE_c$).

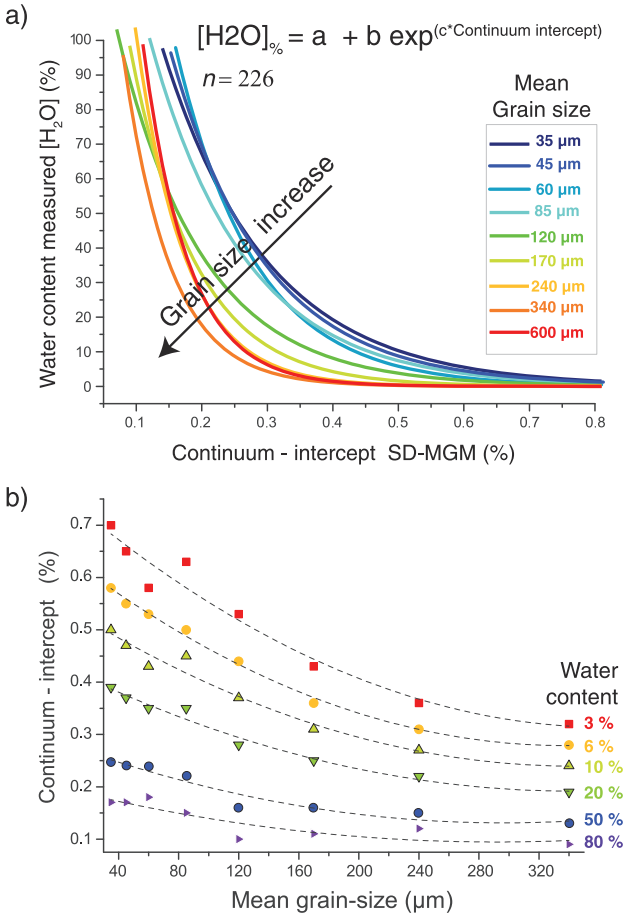

Figure 12. (a) Exponential model used to estimate water content after SD-MGM procedure. *X* axis represents the intercept of the continuum; *Y* axis is the measured water content in the sample for a sand sediment sample. (b) Plot representing the intercept of the continuum deriving from SD-MGM (*Y* axis) versus the mean grain size fractions (*X* axis) for different relative known water content (%).

revealing that the increase in grain size corresponds to a decrease in the continuum intercept during dehydration. This gradient effect is strictly due to grain size changes which are indirectly connected to the porosity or roughness of sand structures as already stated by *Small et al.* [2009]. Such a trend means that grain size changes significantly influence the overall shape of the spectrum during dehydration with a strong nonlinear effect. It is therefore necessary to take sediment grain sizes into account for accurately estimating the water content. Conversely, these results also suggest that the SD-MGM continuum can be used as a good indicator for predicting grain size when water content is known (Figure 12b).

Clearly, both water content and grain size have a nonlinear effect on continuum values (Figures 12a and 12b), which is consistent with the optical theory. Changes in grain size affect surface scattering and the relative proportions of volume scattering to the total observed reflectance. Indeed, an increase in grain size translates into a decrease of the relative proportion of volume scattering [*Hapke*, 1993; *Shkuratov and Gruynko*, 2005].

Variations in accuracy of water and grain size derived from regressions are

tabulated in Table 3. The coefficients of determination (r^2_c) range from 0.75 to 0.96. All nine models developed for the water content retrieval present strong correlation coefficients given a good r^2 ($r^2_{c\text{-mean}} = 0.87$; $n = 226$) among the selected mean grain sizes. Generally, the highest correlations are obtained for fine sediments while coarse sediments show the lowest correlations. We explain these differences by the fact that coarse particles of sands are more likely affected by the rubification phenomenon. In such situation, the broad absorptions of iron oxide observed in the VNIR are well modeled by broad Gaussian distributions (see Figure 6b). For coarser grains, there is a slight shift in the continuum values (see Figure 12, red curve at 600 μm), probably due to the superimposition of the broad ferric absorption band [*Hunt et al*., 1971a].

We have demonstrated using the SD-MGM algorithm not only that an increase of sediment water content has a nonlinear effect on the albedo which is consistent with previous observations [e.g., *Lobell and Asner*, 2002; *Small et al*., 2009] but also that the strength of the water absorption feature at 0.97 μm might be used as an indicator for hydration states. This result also to demonstrate that the SD-MGM continuum is sensitive not only to water content variations but also grain size changes. The SD-MGM deconvolution can be now considered to be a useful technique for isolating water absorption from scattering effects. Results are consistent with the scattering theory for predicting grain size from reflectance spectra [*Hapke*, 1993; *Milliken and Mustard*, 2007a, 2007b]. When a given size category is analyzed separately from the others, the proposed regression models can be independently used to directly estimate grain size fractions in simulated water content scenario. Again, it is possible to separate the contribution of grain size and water content based on continuum and absorption features for a broad size fraction.

6. Discussion

In this section, we will discuss the advantages and limitations of the SD-MGM approach for the retrieval of geophysical properties.

6.1. Consistency of the Proposed Approach

6.1.1. A Comparative Approach for Water-Type Assessments

In the literature, inherent optical properties related to grain size and water content variations are generally well understood, but it is often not possible to separate their respective contributions without some constraints. In most cases, previous investigations focused on band depth and shape of water absorption features in a substrate to predict water content [*Ben-Dor et al*., 1999; *Lobell and Asner*, 2002; *Liu et al*., 2002; *Whiting et al*., 2004; *Adam et al*., 2011], but very few studies have combined both absorption and continuum parameters. *Small et al*. [2009] have already suggested that water content might be distinguished from grain size. Our approach differs from theirs in that it relies on the simultaneous estimation of absorption and continuum parameters derived from the SD-MGM analysis. Such spectral fitting method presents the advantage to be physically based [*Sunshine et al*., 1990]. In the SWIR, the general shape of the spectrum is also controlled by the fundamental water absorption at 2.8 μm. As described previously (see section 2), another comparative spectral fitting method, known as the Soil Moisture Gaussian Model (SMGM; see equation (1)), is better suited for this spectral range [*Whiting et al*., 2004]. In order to independently test consistency and stability of the developed approach, we have directly compared our SD-MGM results with those derived from the SMGM method, applied on the experiment 1 data set.

For water analyses, *Whiting et al*. [2004] used a convex hull also called the "water continuum", extrapolated from the maximum reflectance wavelength to the center of the Gaussian curve at 2.8 μm (Figure 13a). Sediment spectra are fitted by an inverted Gaussian function in the 1.1–2.5 μm spectral range. First, we used the exponential decay function to model the relationships between water content and the fundamental Gaussian band parameter. Second, we scaled the derived Gaussian output parameters provided by both the SD-MGM and the SMGM methods allowing a direct comparison between the derived spectral behaviors (Figure 13b). The distance to the inflection point (σ) or FWHM is found in our case to be the best predictor for water estimates. Note that the strength of the inverted Gaussian function is proportional to FWHM values. In Figure 13b, the overtone band parameter (strength at 0.97 μm) derived from the SD-MGM is directly compared to the fundamental band parameter (FWHM at 2.8 μm) derived from the inverted Gaussian during dehydration. By comparing these two different approaches, it is rather obvious that results exhibit similar trends. Whatever the algorithm used, water types can be perfectly differentiated from each other by the

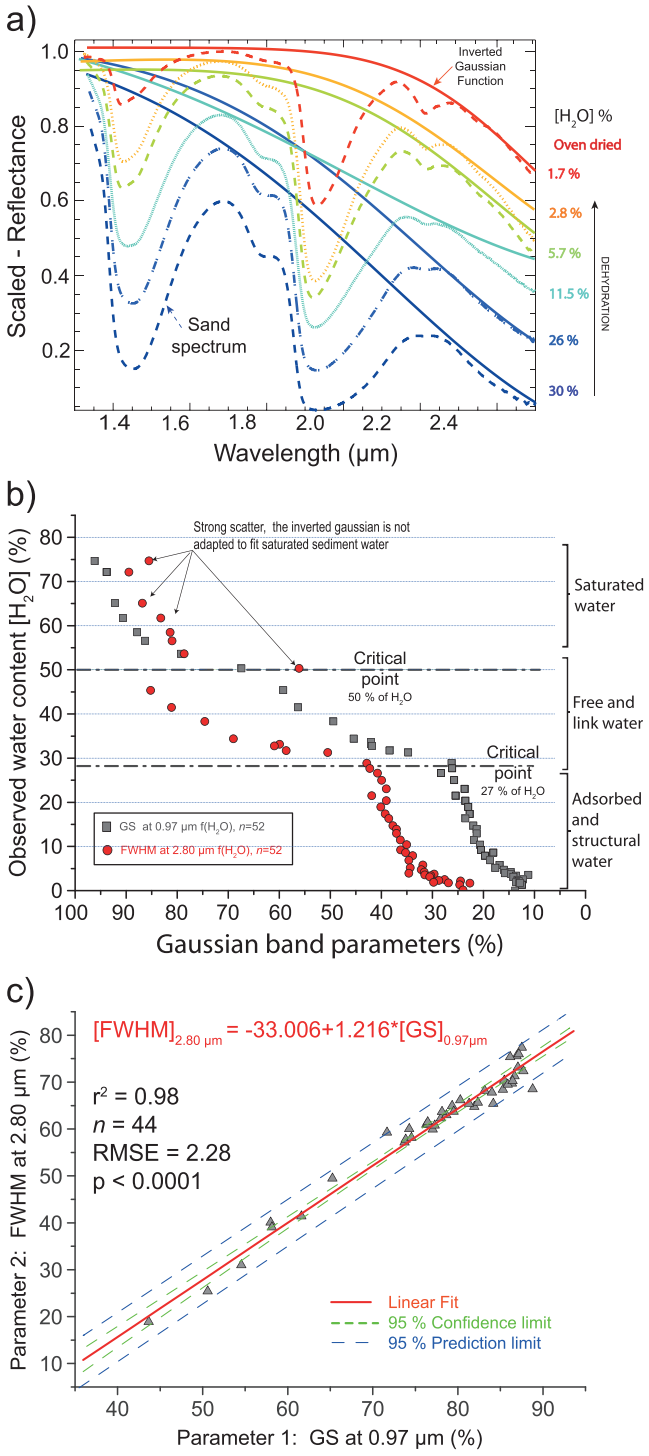

Figure 13. (a) The inverted Gaussian function of sediments is fitted (solid line) to the maximum of the original spectra (dashed line) in the 1.2–2.5 µm spectral range describing a convex hull. (b) Evolution of observed water absorption band parameter (FWHM at 2.8 µm and strength at 0.97 µm). Here the inverted model does not converge for saturated water sediments. (c) Comparison between the strength of absorption parameter at 0.97 µm derived from the SD-MGM and the observed FWHM water content observed at 2.8 µm derived from the SMGM. The relationship is linear. Here saturated water points are masked.

same typical critical limits. Whatever the model used, the limits occur at the same water content level with thresholds estimated around ~ 50% ± 7% and ~ 27 ± 4%. However, although the interstitial water forms are also well identified from SMGM, it is not the case for saturated water. For the saturated water type, the inverted Gaussian model does not converge as indicated by a noncoherent pattern where points are highly scattered and tend to deviate from the regression line (Figure 13b). Hence, we decide to remove from further analyses the saturated measurements. These observations are in agreement with *Lobell and Asner* [2002] who demonstrated the higher sensitivity of the SWIR compared to the VNIR. This greater SWIR sensitivity might be expected from saturated water (~80–65% of H_2O) when the reflectance signal in the SWIR is completely flat or quasi-inexistent (cf. Figure 4a). In Figure 13c, the SD-MGM and SMGM Gaussian parameters are compared together with equivalent water content. A global and positive correlation between the FWHM water absorption band at 2.8 µm and the GS at 0.97 µm is found ($r^2 = 0.98$). Because same results regarding the water forms were obtained with different models, it is reasonable to say that our approach is consistent at least for nonsaturated water content.

6.1.2. Interpretation of the Water-Type Retrieval

Concerning the water type hypothesis, *Small et al*. [2009] have already observed a darkening effect in the final stages of dehydration suggesting that the reflectance variation was neither purely linear [*Idso et al*., 1975] nor purely exponential [*Lobell and Asner*, 2002]. But they proposed an explanation for the nonlinearity by various phases of evaporation at the sample surface. Using another data set, *Rainey et al*. [2000] have plotted measured moisture against reflectance values for various sediments and grain sizes. Although they used a linear regression model, it seems that the spectral behavior in response to hydration changes might be nonlinear.

When looked at in more details, their results might also exhibit three separate sections that could be attributed to saturated, free, and adsorbed water. Similarly, *Adam et al*. [2011] plotted the relative moisture content of sediment samples versus the scaled band area at 1.425 μm. They predicted water content by fitting the data with two different second-order polynomial models and a critical point at 20% of water. Their results also revealed two separate sections that could be attributed to saturated and interstitial water. Note that *Adam et al*. [2011] mentioned that for water content larger than 20%, a thin layer of water was visible at the surface. In Figure 9a, two critical points are encountered: one between free water and adsorbed water (~27 ± 4%) and another one between free water and saturated state (~50 ± 7%). Critical point positions can be explained by a modification of the scattering processes due to water within macropore and micropore and around grain surfaces at this particular sediment moisture level. One could argue that these threshold values might depend on the number of measurements, but it is easy to see on Figures 9 and 13 that the "transition" zones are covered by enough measurements to be clearly identified. Moreover, the existence of a critical point has already been pointed out by *Liu et al*. [2002]. These authors interpreted this critical point as related to the hydrodynamic characteristics of the soils with its position depending on soil types.

We assume that the reflectance pattern is mostly driven by the water type and that the multiple nonlinear exponential model regression between moisture content and strength at 0.97 μm appears as the most promising spectral criterion to separate water forms. Note that this water-type pattern is certainly a function of compositional changes. For example, we might expect that a sample mainly composed of wet mud with high clay content might show a different pattern than the one we proposed because the porosity and permeability are totally different. It is expected that modifications may occur on both the degrees of nonlinearity and the critical limits between water types. The limits between water types should be highly dependent on sediment types (i.e., sand and mud) and kinetics forces of fixation/removal. These limits are not strictly fixed to a precise absorption depth value or a reflectance value [see *Rainey et al*., 2000]. However, more controlled laboratory experiments are needed to extend the range of our observations and provide some clues about water type for a clay sediment composition. As our study is based on a limited number of sediment types, performing additional measurements on various sediment types should provide a complete understanding of water forms following their water potential exchange, retention capacity, and porosity as a function of sediment type. In another context, the water adsorption and desorption was already studied by *Pommerol et al*. [2009]. As mentioned before, our proposed approach reveals less accurate water prediction for low water content (<3.5%).

6.1.3. A Comparative Approach for the Water Continuum Assessments

In this study, the continuum is used as a proxy for geophysical properties. In order to test the consistency of our method to predict water content from the SD-MGM continuum, we compared our results to the SMGM approach. Similarly, during dehydration, we compared the value of the continuum intercept derived from the SD-MGM to the slope of the inverted Gaussian model (Figure 14a). The resulting plot exhibits quite similar monotonic negative trend during dehydration. We observe that an increase of water content causes a decrease of the continuum and slope parameters for similar grain size. SD-MGM continuum and slope of the inverted Gaussian are directly compared in Figure 14b, showing a strong linear correlation ($r^2 = 0.99$) and consistencies between models. Hence, the SD-MGM can be used as a water indicator. Compared to Gaussian changes during dehydration process, it is not possible to identify the different hydration states from the variation of the continuum parameters. Monotonic behavior is explained by the fact that the continuum of reflectance is fitted over a broader spectral range as opposed to the Gaussian fitting range.

6.1.4. Interpretation of the Continuum as a New Indicator of Geophysical Properties

We selected a modeled continuum, the MGM continuum previously described, instead of the standard continuum elaborated by *Clark and Roush* [1984], because it is more consistent with scattering processes [see *Sunshine et al*., 1990]. The standard continuum elaborated by *Clark and Roush* [1984] is not suited for our application because in certain cases it generates false absorption bands with no spectral significance. For example, such artifact may appear at the edge of the spectral window. Whereas using SD-MGM analysis all absorption bands are well modeled by Gaussian profiles, resulting in a good estimation of the continuum shape. Hence, the SD-MGM continuum can be interpreted as the part of the spectrum which is not explained by absorption bands such as the scattering function. Of course, although the MGM functions (i.e., Gaussian and continuum) used here seem to be appropriate for modeling physical processes, some uncertainties may remain following the choice of the mathematical function type. Traditional spectral band analyses are

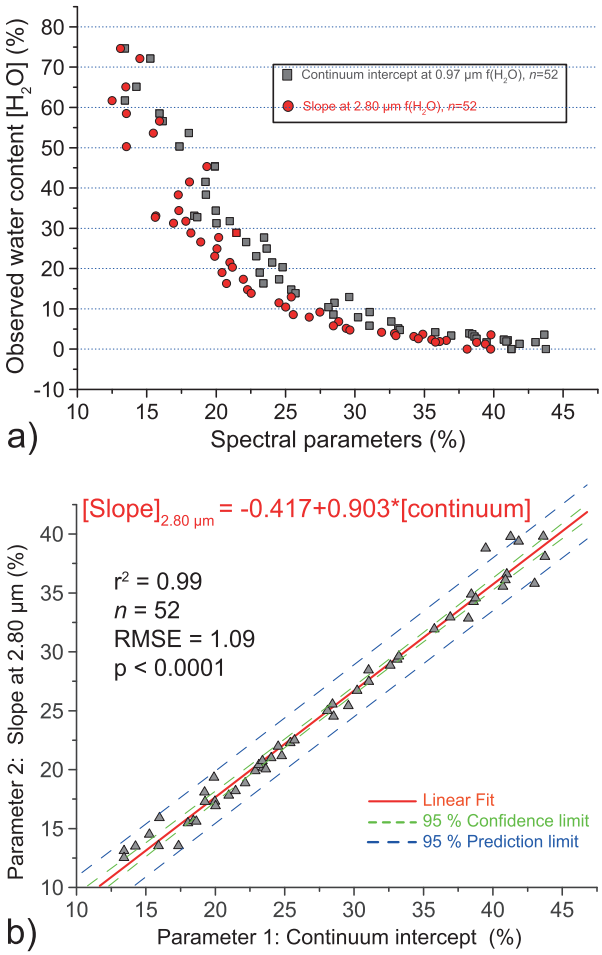

Figure 14. (a) Evolution of the continuum intercept derived from the previous model regression of the SD-MGM and the slope of the Inverted Gaussian at 2.8 µm derived from the SMGM during dehydration. (b) Comparison between the intercept continuum and the slope of the Inverted Gaussian. The relationship is linear.

usually limited due to the limited number of available bands while hyperspectral data offer the possibility to assess the overall shape of the spectrum. Here the SD-MGM has the great advantage to integrate the whole spectral range through the deconvolution process. Consequently, the derived regression techniques are less biased than the regression performed from band ratio or spectral index for instance.

The SD-MGM continuum can be used as an indicator for moisture content. This observation is in agreement with those reported by *Lobell and Asner* [2002], *Liu et al.* [2002], and *Whiting et al.* [2004]. It has already been suggested that the lower reflectance values which are translated into low continuum value are associated with an increase in water content. This observation is corroborated by a decrease of the relative refractive index of the medium surrounding the sediment particles as a result of water replacing air [*Twomey et al.*, 1986].

The impact of grain size variations on laboratory spectra has already been studied by a number of authors including *Clark and Roush* [1984], *Hapke* [1993], *Lucey* [1998], *Milliken and Mustard*, 2007a, 2007b, and *Pommerol and Schmitt* [2008a]. It has already been shown that smaller grains may result in higher absolute reflectance values [*Adams and Filice*, 1967; *Mustard and Hays*, 1997]. Focusing on grain size analyses (experiment 2), it was shown that whatever the selected grain size, the continuum values decreased with dehydration (see Figure 12a). For a given water content, the decrease in grain size is associated with the increase in continuum values (see Figure 12b). These spectral effects are proved to be nonlinear. Coarse and dry sediments seem to have a stronger effect on continuum values (strong curvature) than fine and wet sediments. *Zhu et al.* [2010] mentioned that during dehydration the grain size of sand has a strong effect on soil reflectance patterns. We demonstrated that grain size changes have a nonnegligible effect on sand spectra even during dehydration which is consistent with the scattering theory. With the exception of complex radiative transfer approaches, limitations to predicting grain size are explained by the difficulty in separating scattering from absorption in the overall spectral shape. The exponential decay function is used to fit the data for each fraction size but with different coefficients for different size (cf. Figure 12). *Lucey* [1998] showed that scattering theory predicts that single-scattering albedo also decreases exponentially with grain size. Scattering theory predicted that spectral contrast of absorption bands was dependent on both mean path length and absorption coefficient. Note that the eventual change in the composition would also have an effect on the coefficients. Without the knowledge of the absorption coefficient or the grain size distribution in bulk sediment, it is not possible to separate the respective contributions of albedo and grain size from the spectral contrast changes (scattering) of the hydration band [*Milliken and Mustard*, 2007a, 2007b]. For grain size analyses, additional data with

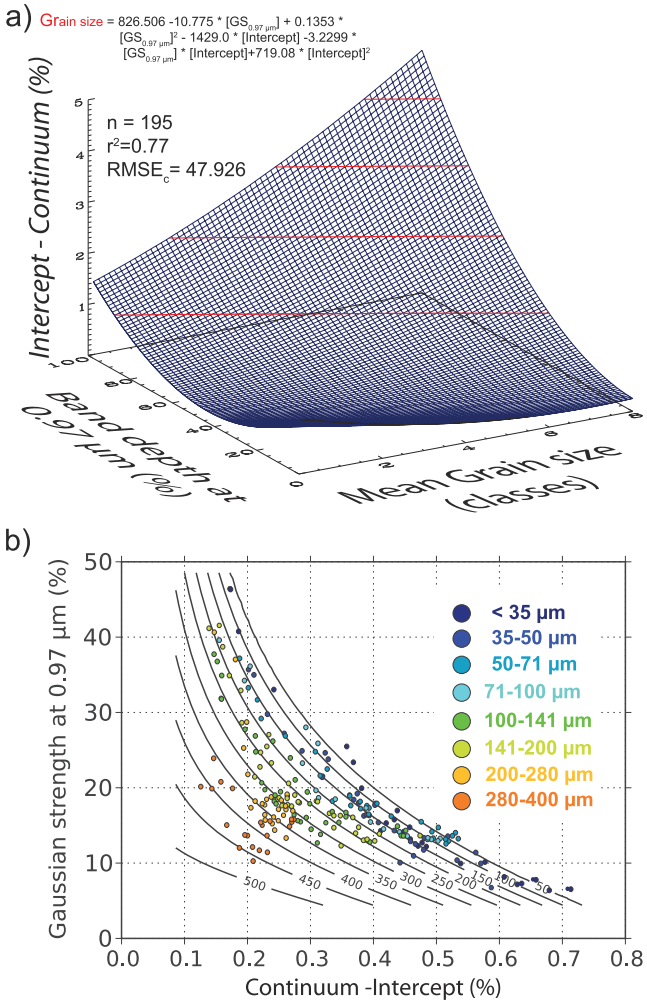

Figure 15. (a) Three-dimensional representation of the separability of the mean grain size during dehydration. The full hyperbolic model is used to estimate grain size after SD-MGM process (blue curve). *X* axis is the estimation of the band depth at 0.97 µm, *Y* axis is the measured particle size in a sand sediment samples, and *Z* axis is the estimation of the continuum (intercept). (b) Contour plot after data interpolation.

different composition of sediments (e.g., minerals and pigments) are desirable to determine if the exponential curve is unique or sample-specific.

6.2. Implications and Perspectives for Future Coastal Studies

One of the fundamental challenges in coastal remote sensing applications is to understand the spectral features characteristics and their connections with sedimentary parameters. In nature, sediment parameters are from an environmental point of view closely interrelated [*Deronde et al*., 2006; *Choi et al*., 2010]. Therefore, hyperspectral remote sensing data can be a useful tool to retrieve biogeophysical properties of sediments such as grain size and water content [*Bryant et al*., 1996; *Carrère et al*., 2004; *Smith et al*., 2004; *Deronde et al*., 2006; *Combe et al*., 2005; *van der Wal and Herman*, 2007; *Verpoorter et al*., 2009]. *Small et al*. [2009] suggested that if it was possible to separate effect of grain size from moisture content, it should be possible to map sediment composition and water content at synoptic scales using hyperspectral data.

Although, in laboratory conditions, it is common to analyze specific hydration absorption overtones at 1.40 and 1.90 µm to predict liquid water content, this is not possible when using field measurements or hyperspectral images since these absorptions are also strongly affected by atmospheric water vapor which are saturated and therefore mask the liquid water absorptions. However, liquid water absorptions at 0.97 µm and 1.20 µm may be fully used to derive water content for field and image analyses because the water vapor absorptions at 0.94 µm, 1.14 µm, and 1.38 µm are not saturated and hence have a lower impact on the liquid water bands [*Eldridge*, 1967; *Kratz and Cess*, 1985]. Even though continuum analysis does not give access to the information about the different water types, it appears to be a promising way to predict and map water content by minimizing the atmospheric effect.

We propose to merge the relevant spectral information presented in this study into a 3-D regression model. Such a model appears to be useful for grain size retrieval as it constitutes a single prediction model and might be easily applied to a hyperspectral image for instance. This preliminary model has been applied to the material of experiment 2. In Figures 15a and 15b, the continuum intercept (*Z* axis) is regressed as a function of Gaussian strength at 0.97 µm (*X* axis) versus the experimental grain size fractions (*Y* axis). Because Gaussian and continuum parameters can be derived from each pixel of the image [*Combe et al*., 2005] and are consequently known, it becomes also possible to retrieve the mean grain size for each pixel ($M\Phi$).

Various predicted 3-D models were tested on this spectral data set (e.g., polynomial, exponential, and logarithmic). The best model is chosen based on the r^2 and complementary error statistic, including the $RMSE_c$. Among the tested equations, several models show low $RMSE_c$ and therefore are a potential candidates, for example, simplified quadratic exponential transform ($RMSE_c = 47.66$), full quadratic exponential transform ($RMSE_c = 47.90$), full quadratic ($RMSE_c = 47.92$), or simplified quadratic logarithmic transform ($RMSE_c = 47.94$). With a lower number of coefficients, the full quadratic model appears to be a reasonable model for grain size estimation with respect to spectral evolution during dehydration. The relationship for mean grain size ($M\Phi$) estimation is presented below:

$$M\Phi = 826.506 - 10.775\left[GS_{0.97\mu m}\right] + 0.1353\left[GS_{0.97\mu m}\right]^2 - 1429[IC] - 3.229\,[IC]\left[GS_{0.97\mu m}\right] + 719.08[IC]^2 \quad (4)$$

where $M\Phi$ is the mean grain size, $GS_{0.97}$ the Gaussian strength at 0.97 μm, and IC the intercept of the SD-MGM continuum. By simultaneously considering these three parameters within the full quadratic model (equation (4)), it is possible to separate the surface texture from spectral surface observations ($r^2 = 0.41$; $n = 226$; nine fraction sizes). Low r^2 related to coarse grains might be due to the presence of an iron oxide absorption. Notice that there is a significant improvement of the r^2 when the 400–800 μm fraction size is removed from the calibration data set ($r^2 = 0.77$; $n = 195$; eight fraction sizes).

The obtained experimental results indicate that it is possible to treat simultaneously the effects of variations of continuum reflectance and absorption bands to retrieve quantitative information on water content and grain size from experimental reflectance measurements, but, when applied to an image, such model presents some limitations. *Rainey et al*. [2000] showed that the spectral contrast between coarse and fine intertidal sediments was primarily a product of their very different spectral responses to moisture loss. But, as pointed out by *Small et al*. [2009], natural surfaces are spectrally diverse and complex; grain size and water content are not the only parameters which influence the spectral behavior. In natural conditions, additional difficulties to treat simultaneously these effects may appear by considering the wide variability in geophysical properties and compositions of coastal sediments. For example, concerning the other coastal environments such as macrotidal beaches, the grain size of the intertidal sediments may vary from well sorted to poorly sorted. Additional research is required to extend and test the sediment moisture sensitivity analyses with respect to viewing geometry and sediment roughness for instance. Regarding the possible generalization of the proposed method in natural environment, further investigations are certainly necessary to better assess the impact of sorting on the surface roughness properties and then on both the continuum of reflectance and strength of the absorptions. Similarly, it would be interesting to study the impact of high organic matter [*Baumgardner et al*., 1970; *Ben-Dor et al*., 1999] or high carbonate contents on the overall shape of the spectrum and also the presence of microphytobenthos on the absorption band occurrence by using the SD-MGM approach. Hence, it is clear that additional assessments are desirable to be fully reproducible to a wide range of coastal environments. Nevertheless, integrating the proposed overall approach for coastal applications would open interesting perspectives for mapping geophysical properties of sediment such as grain size and water content. Removing the spectral effect of water in sediments is primarily to better constrain the effects of particle size, surface roughness, mineral composition, and organic matter content. In another context, our optimization algorithm (SD-MGM) combined with appropriate experimental measurements have potentially strong implications for a large variety of coastal research. Particularly, mapping the mean grain size as well as separating "wet" and "dry" areas on a pixel-by-pixel basis from hyperspectral images will provide some important clues for many coastal applications and coastal management including stabilization of mudflats, beach nourishment projects, coastal protection design, calibration and verification of hydrodynamic models or suspension models for shellfish applications, nature preservation, and finally the examination of boundary properties for coastal development regulation policies. The process of sediment transport and deposition is strongly dependent on the biogeophysical properties. Grain size is a fundamental property of any sediment, which can provide important clues to nature, sediment source, entrainment, transport history, and depositional conditions. Grain size and water content maps offer the possibility to predict erodibility of sediments.

7. Conclusion

This paper demonstrates that it is now possible to separate water content from grain size spectral effect, within the context of applications to intertidal surfaces such as Bourgneuf Bay. This paper presents new results from laboratory investigations and a physically based spectral fitting algorithm to retrieve water content and grain size from spectral data. We have demonstrated the value of qualitative and quantitative sediment characteristics using spectral feature extractions from continuum and absorption in combination with sedimentological measurements and SD-MGM algorithm procedure. Results show strong correlations between absorption strength at 0.97 μm and continuum intercept as derived from SD-MGM, and water content demonstrating the ability to successfully quantify water abundance using predictive models. Although both spectral parameters show respectively strong correlation coefficients ($r^2_{c\text{-mean}} = 0.96$ and $r^2 = 0.98$, respectively), more accurate predictions are obtained using the absorption feature rather than the continuum, including the possibility to discriminate different hydration states (i.e., saturated, free, and adsorbed water). Although the continuum variations do not exhibit the same trend, they appear to be a useful indicator because less dependent on specific liquid water absorption bands which are often masked by atmospherical effects in natural conditions.

In this study, we have also investigated the consistency of our results by comparing them to another spectral fitting method, the Soil Moisture Gaussian Model (SMGM) of *Whiting et al*. [2004] which uses the fundamental water absorption band at 2.8 μm. The derived SMGM results show a good consistency with the SD-MGM results. We also derived original results from the use of reflectance continuum characteristics to estimate water content. Finally, we have shown that the SD-MGM continuum could be used as an indicator of grain size. It is important to separate the contribution of grain size and water on continuum and absorption parameters. We have presented a new and promising approach regarding the estimation of grain size during dehydration from siliceous materials while taking into account the spectral effect of grain size and water in the VNIR spectral range. These results proved to be consistent with absorption/scattering theory.

Acknowledgments
This paper based on research was in partly funded by the BQR ULCO 2014, bonus qualité recherche 2014 of the Université du Littoral Côte d'Opale (ULCO).

References

Adam, S., A. De Backer, A. De Wever, K. Sabbe, E. A. Toorman, M. Vincx, and J. Monbaliu (2011), Bio-physical characterization of sediment stability in mudflats using remote sensing: A laboratory experiment, *Cont. Shelf Res.*, *31*(10), S26–S35, doi:10.1016/j.csr.2009.12.008.

Adams, J. B., and A. L. Filice (1967), Spectral reflectance 0.4 to 2.0 microns of silicate rock powders, *J. Geophys. Res.*, *72*(22), 5705–5715, doi:10.1029/JZ072i022p05705.

Ångström, A. (1925), The albedo of various surfaces of ground, *Geograpfiske Annaler*, *7*, 323–342.

Baumgardner, M., L. Silva, L. Biehl, and E. Stoner (1986), Reflectance properties of soils, *Adv. Agron.*, *38*, 1–44, doi:10.1016/S0065-2113(08)60672-0.

Baumgardner, S. J., M. F. Kristof, and A. L. Zachary (1970), Effects of organic matter on multispectral properties of soils, *Proc. Indiana Acad. Sci.*, *79*, 413–422.

Bedidi, A., B. Cervelle, J. Madeira, and M. Pouget (1992), Moisture effects on visible spectral characteristics of lateritic soils, *Soil Sci.*, *153*(2), 129–141.

Ben-Dor, E., J. R. Irons, and G. F. Epema (1999), Soil reflectance, in *Remote Sensing for Earth Sciences: Manuel of Remote Sensing*, edited by A. N. Rencz, pp. 11–188, Wiley, New York.

Ben-Dor, E., N. Levin, A. Singer, A. Karnieli, O. Braun, and G. J. Kidron (2006), Quantitative mapping of the soil rubification process on sand dunes using an airborne hyperspectral sensor, *Geoderma*, *131*, 1–21, doi:10.1016/j.geoderma.2005.02.011.

Blott, S. J., and K. Pye (2001), GRADISTAT: A grain-size distribution and statistics package for the analysis of unconsolidated sediments, *Earth Surf. Processes Landforms*, *26*, 1237–1248, doi:10.1002/esp.261.

Bowers, S. A., and R. J. Hanks (1965), Reflection of radiant energy from soils, *Soil Sci. Soc. Am. J.*, *100*, 130–138.

Bryant, R., A. Tyler, D. Gilvear, P. McDonald, I. Teasdale, J. Brown, and G. Ferrier (1996), A preliminary investigation into the spectral characteristics of inter-tidal estuarine sediments, *Int. J. Remote Sens.*, *17*(2), 405–412, doi:10.1080/01431169608949016.

Carrère, V., N. Spilmont, and D. Davoult (2004), Comparison of a simple techniques for estimating chlorophyll a concentration in the intertidal zone using spectral-resolution field spectrometer data, *Mar. Ecol. Prog. Ser.*, *274*, 31–40, doi:10.3354/meps274031.

Choi, J.-K., J.-H. Ryu, H.-R. Yoo, H.-J. Woo, and C. H. Kim (2010), Quantitative estimation of intertidal sediment characteristics using remote sensing and GIS, *Estuarine Coastal Shelf Sci.*, *88*, 125–134, doi:10.1016/j.ecss.2010.03.019.

Clark, R. N. (1999), Spectroscopy of rocks and minerals, and principle of spectroscopy, in *Remote Sensing for the Earth Sciences: Manual of Remote Sensing*, edited by N. Rencz, pp. 3–52, John Wiley, New York.

Clark, R. N., and T. L. Roush (1984), Reflectance spectroscopy: Quantitative analysis techniques for remote sensing applications, *J. Geophys. Res.*, *89*, 6329–6340, doi:10.1029/JB089iB07p06329.

Collins, J. R. (1937), The near infrared absorption band of liquid water at 1.79 μm, *Phys. Rev.*, *52*(2), 88–90, doi:10.1103/PhysRev.52.88.

Combe, J. P., P. Launeau, V. Carrère, D. Despan, V. Méléder, L. Barillé, and C. Sotin (2005), Mapping microphytobenthos biomass by non-linear inversion of visible-infrared hyperspectral images, *Remote Sens. Environ.*, *98*, 371–387, doi:10.1016/j.rse.2005.07.010.

Demetriades-Shah, T. H., M. D. Steven, and J. A. Clark (1990), High resolution derivative spectra in remote sensing, *Remote Sens. Environ.*, *33*(1), 55–64, doi:10.1016/0034-4257(90)90055-Q.

Deronde, B., P. Kempeneers, and R. Forster (2006), Imaging spectroscopy as a tool to study sediment characteristics on a tidal sandbank in the Westerschelde, *Estuarine Coastal Shelf Sci.*, *69*, 580–590, doi:10.1016/j.ecss.2006.05.048.

Dixit, L., and S. Ram (1985), Quantitative analysis by derivative electronic spectroscopy, *Appl. Spectrosc. Rev.*, *21*(4), 311–418, doi:10.1080/05704928508060434.

Dolgov, S. I., and G. B. Vinogradova (1973), Reflection coefficient of moist soils, *Soviet Soil Sci.*, *5*, 735–737.
Eldridge, R. G. (1967), Water vapor absorption of visible and near infrared radiation, *Appl. Opt.*, *6*(4), 79–713, doi:10.1364/AO.6.000709.
Faraji, H., T. Crowe, R. Besant, S. Sokhansanj, and H. Wood (2004), Prediction of moisture content potash fertilizer using NIR spectroscopy, *Can. Biosyst. Eng.*, *46*, 345–348.
Gaffey, S., L. A. McFadden, D. Nash, and C. M. Pieters (1993), Ultraviolet, visible, and near-infrared reflectance spectroscopy: Laboratory spectra of geologic materials, in *Remote Geochemical Analysis: Elemental and Mineralogical Composition*, edited by C. M. Pieters and P. A. J. Englert, pp. 43–78, Cambridge Univ. Press, Cambridge, U. K.
Goodin, D. G., L. Han, R. N. Fraser, D. C. Rundquist, W. A. Stebbins, and J. F. Schalles (1993), Analysis of suspended solids in water using remotely sensed high resolution derivative spectra, *Photogramm. Eng. Remote. Sens.*, *59*, 505–510.
Gouleau, D. (1968), Etude hydrologique et sédimentologique de la baie de Bourgneuf PhD thesis, Thèse de 3ème cycle, Univ. de Nantes, 85 pp., Nantes.
Gouleau, D. (1975), Les premiers stades de la sédimentation sur les vasières littorales Atlantiques rôle de l'émersion PhD thesis, Thèse d'Etat, université de Nantes, 242 p+ annexes, Nantes.
Hapke, B. (1993), *Theory of Reflectance and Emittance Spectroscopy*, 455 pp., Cambridge Univ. Press, New York.
Hœpffner, N., and S. Sathyendranath (1991), Effect of pigment composition on absorption properties of phytoplankton, *Mar. Ecol. Prog. Ser.*, *73*, 11–23, doi:10.1364/OE.20.011882.
Huguenin, R. L., and J. L. Jones (1986), Intelligent information extraction from reflectance spectra: Absorption band positions, *J. Geophys. Res.*, *91*, 9585–9598, doi:10.1029/JB091iB09p09585.
Hunt, G., and J. Salisbury (1970), Visible and near-infrared spectra of minerals and rocks. I. Silicate minerals, *Mod. Geol.*, *2*, 283–300.
Hunt, G., J. Salisbury, and C. Lenhoff (1971a), Visible and near-infrared spectra of minerals and rocks. III. Oxides and hydroxides, *Mod. Geol.*, *2*, 195–205.
Idso, S. B., D. R. Jackson, R. J. Reginato, B. A. Kimball, and F. S. Nakama (1975), The dependence of bare soil albedo on soil water content, *J. Appl. Meteorol.*, *14*, 109–113, doi:10.1175/1520-0450(1975)014<0109:TDOBSA>2.0.CO;2.
Ishida, T., H. Ando, and M. Fukuhara (1991), Estimation of complex refractive index of soil particles and its dependence on soil chemical properties, *Remote Sens. Environ.*, *38*(3), 173–182, doi:10.1016/0034-4257(91)90087-M.
Kanner, L. C., J. F. Mustard, and A. Gendrin (2007), Assessing the limits of the Modified Gaussian Model for remote spectroscopic studies of pyroxenes on Mars, *Icarus*, *187*(2), 442–456, doi:10.1016/j.icarus.2006.10.025.
Kratz, D. P., and R. D. Cess (1985), Solar absorption by atmospheric water vapor: A comparison of radiations models, *Tellus*, *37B*, 53–63, doi:10.1111/j.1600-0889.1985.tb00055.x.
Le Hir, P., W. Roberts, O. Cazaillet, M. Christie, P. Bassoullet, and C. Bacher (2000), Characterization of intertidal flat hydrodynamics, *Cont. Shelf Res.*, *20*, 1079–1097, doi:10.1016/S0278-4343(00)00031-5.
Liu, W., F. Baret, X. Gu, Q. Tong, L. Zheng, and B. Zhang (2002), Relating soil surface moisture to reflectance, *Remote Sens. Environ.*, *81*(2–3), 238–246, doi:10.1016/S0034-4257(01)00347-9.
Lobell, D. N., and G. P. Asner (2002), Moisture effects on soil reflectance, *Soil Sci. Soc. Am.*, *66*, 722–727, doi:10.2136/sssaj2002.7220.
Lucey, P. G. (1998), Model near-infrared optical constants of olivine and pyroxene as a function of iron content, *J. Geophys. Res.*, *103*, 1703–1713, doi:10.1029/97JE03145.
Massé, M., O. Bourgeois, S. Le Mouélic, C. Verpoorter, L. Le Deit, and J. P. Bibring (2010), Martian polar and circum-polar sulfate-bearing deposits: Sublimation tills derived from the North Polar Cap, *Icarus*, *209*(2), 434–451, doi:10.1016/j.icarus.2010.04.017.
Massé, M., O. Bourgeois, S. Le Mouélic, C. Verpoorter, A. Spiga, and L. Le Deit (2011), Wide distribution and glacial origin of polar gypsum on Mars, *Earth Planet. Sci. Lett.*, *317–318*, 44–55, doi:10.1016/j.epsl.2011.11.035.
Milliken, R. E., and J. F. Mustard (2005), Quantifying absolute water content of minerals using near-infrared reflectance spectroscopy, *J. Geophys. Res.*, *110*, 1–25, doi:10.1029/2005JE002534.
Milliken, R. E., and J. F. Mustard (2007a), Estimating the water content of hydrated minerals using reflectance spectroscopy: I. Effects of darkening agents and low-albedo materials, *Icarus*, *189*, 550–573, doi:10.1016/j.icarus.2007.02.017.
Milliken, R. E., and J. F. Mustard (2007b), Estimating the water content of hydrated minerals using reflectance spectroscopy: II. Effects of particle size, *Icarus*, *189*, 574–588, doi:10.1016/j.icarus.2006.12.028.
Mustard, J. F., and J. E. Hays (1997), Effect of hyperfine particles on reflectance spectra from 0.3 to 25 μm, *Icarus*, *125*, 145–163, doi:10.1006/icar.1996.5583.
Mustard, J. M., S. Murchie, S. Erard, and J. Sunshine (1997), In situ compositions of Martian volcanics implication for the mantle, *J. Geophys. Res.*, *102*(E11), 25,605–25,615, doi:10.1029/97JE02354.
Noble, S. K., C. Pieters, T. Hiroi, and A. Taylor (2006), Using the modified Gaussian model to extract quantitative data from lunar soils, *J. Geophys. Res.*, *11*, E11009, 1–17, doi:10.1029/2006JE002721.
Painter, T. H., N. P. Molotch, M. Cassidy, M. Flanner, and K. Steffen (2007), Instruments and methods. Contact spectroscopy for determination of stratigraphy of snow optical grain size, *J. Glaciol.*, *53*, 180.
Peterson, J. B., B. F. Robinson, and R. H. Beck (1979), Predictability of change in soil reflectance on wetting, in *Proc. Symp. Machine Processing of Remotely Sensed Data*, 5th ed., edited by I. M. Tendam and D. B. Morrison, pp. 264–272, West Lafeyette, IN Lars Technical Report 062479.
Philpot, W. D. (1991), The derivative ratio algorithm: Avoiding atmospheric effects in remote sensing, *IEEE Trans. Geosci. Remote Sens.*, *29*, 350–357, doi:10.1109/36.79425.
Pieters, C. (1983), Strength of mineral absorption features in the transmitted component of near-infrared reflected light: First results from RELAB, *J. Geophys. Res.*, *88*(11), 9534–9544, doi:10.1029/JB088iB11p09534.
Pommerol, A., and B. Schmitt (2008a), Strength of the H_2O near-infrared absorption bands in hydrated minerals: Effects of particle size and correlation with albedo, *J. Geophys. Res.*, *113*, E10009, doi:10.1029/2007JE003069.
Pommerol, A., and B. Schmitt (2008b), Strength of the H_2O near-infrared absorption bands in hydrated minerals: Effects of measurement geometry, *J. Geophys. Res.*, *113*, E10009, doi:10.1029/2008JE003197.
Pommerol, A., B. Schmitt, P. Beck, and O. Brissaud (2009), Water sorption on Martian regolith analogs: Thermodynamics and near-infrared reflectance spectroscopy, *Icarus*, *204*, 114–136, doi:10.1016/j.icarus.2009.06.013.
Rainey, M. P., A. N. Tyler, R. G. Bryant, D. J. Gilvear, and P. Mc Donald (2000), The influence of surface and interstitial moisture on the spectral characteristics of intertidal sediments: Implications for airborne image acquisition and processing, *Int. J. Remote Sens.*, *21*, 3025–3038, doi:10.1080/01431160050144938.
Rainey, M. P., A. N. Tyler, R. G. Bryant, D. J. Gilvear, and P. Mc Donald (2003), Mapping intertidal estuarine sediment grain-size distributions through airborne remote sensing, *Remote Sens. Environ.*, *86*, 480–490, doi:10.1016/S0034-4257(03)00126-3.
Rodger, A., C. Laukamp, M. Haest, and T. Cudahy (2012), A simple quadratic method of absorption feature wavelength estimation in continuum removed spectra, *Remote Sens. Environ.*, *118*, 273–283, doi:10.1016/j.rse.2011.11.025.

Savitzky, A., and M. E. J. Golay (1964), Smoothing and differentiation of data by simplified least squares procedures, *Anal. Chem.*, *36*, 1627–1639, doi:10.1021/ac60214a047.

Shkuratov, Y. G., and Y. S. Gruynko (2005), Light scattering by media composed of semitransparent particles of different shapes in ray optics approximation: Consequences for spectroscopy, photometry, and polarimetry of planetary regoliths, *Icarus*, *173*, 16–28, doi:10.1016/j.icarus.2003.12.022.

Small, C., M. Steckler, L. Seeber, S. H. Akhter, S. Goodbred, B. Mia, and B. Imam (2009), Spectroscopy of sediments in the Ganges-Bahmaputra: Spectral effects of moisture, grain size and lithology, *Remote Sens. Environ.*, *113*, 342–361, doi:10.1016/j.rse.2008.10.009.

Smith, G., A. Thomson, I. Moller, and J. Kromkamp (2004), Using hyperspectral imaging for the assessment of mudflat surface stability, *J. Coastal Res.*, *20*(4), 1165–1175, doi:10.2112/03-0039R.1.

Suehara, K.-I., Y. Ohta, Y. Nakano, and T. Yano (1999), Rapid measurement under control of the moisture content of compost using near-infrared spectroscopy, *J. Biosci. Bioeng.*, *87*(6), 769–774, doi:10.1016/S1389-1723(99)80151-0.

Sunshine, J. M., and C. M. Pieters (1993), Estimating modal abundances from the spectra of natural and laboratory pyroxene mixtures using the modified Gaussian model, *J. Geophys. Res.*, *95*, 9075–9087, doi:10.1029/93JE00677.

Sunshine, J. M., C. M. Pieters, and S. F. Pratt (1990), Deconvolution of mineral absorption bands: An improved approach, *J. Geophys. Res.*, *95*(B5), 6955–6966, doi:10.1029/JB095iB05p0695.

Talsky, G. (1994), *Derivative Spectrophotometry. Low and Higher Order*, VCH Publishers, Inc., New York.

Tarantola, A., and B. Valette (1982), Generalized nonlinear inverse problems solved using the least squares criterion, *Rev. Geophys.*, *20*, 219–232, doi:10.1029/RG020i002p00219.

Tsai, F., and W. Philpot (1998), Derivative analysis of hyperspectral data, *Remote Sens. Environ.*, *66*, 41–51, doi:10.1016/S0034-4257(98)00032-7.

Twomey, S. A., C. F. Bohren, and J. L. Mergenthaler (1986), Reflectance and albedo differences between wet and dry surfaces, *Appl. Opt.*, *25*, 431–437, doi:10.1364/AO.25.000431.

van der Wal, D., and P. Herman (2007), Regression-based synergy of optical, shortwave infrared and microwave remote sensing for monitoring the grain-size of intertidal sediments, *Remote Sens. Environ.*, *111*(1), 89–106, doi:10.1016/j.rse.2007.03.019.

Verpoorter, C. (2009), Télédétection hyperspectrale et cartographie des faciès sédimentaires en zone intertidale. Application à la Baie de Bourgneuf PhD thesis, Nantes Univ., 423 p., Ed Universitaire Européenne.

Verpoorter, C., V. Carrère, and M. Robin (2007), Retrieval of physical properties of mudflat sediments from hyperspectral data using the Modified Gaussian Model and spectral curve fitting, in *Proceedings of the 5th EARSeL SIG IS Workshop on Imaging Spectroscopy*, 10 pp., EARSeL, Bruges, Belgium.

Verpoorter, C., V. Carrère, and J.-P. Combe (2009), Sediment characterization in the intertidal zone of the Bourgneuf Bay (France) using the Automated Modified Gaussian Model (SD-MGM), in *Proceedings of the 6th EARSeL SIG Imaging Spectroscopy Workshop*, 6 pp., EARSeL, Tel-Aviv, Israel.

Whiting, M. L., L. Li, and S. L. Ustin (2004), Predicting water content using Gaussian model on soil spectra, *Remote Sens. Environ.*, *89*(4), 535–552, doi:10.1016/j.rse.2003.11.009.

Yen, A. S., B. C. Murray, and G. R. Rossman (1998), Water content of the Martian soil: Laboratory simulations of reflectance spectra, *J. Geophys. Res.*, *103*, 11,125–11,134, doi:10.1029/98JE00739.

Zhu, Y., D. C. Weindorf, S. Chakraborty, B. Haggard, S. Johnson, and N. Bakr (2010), Characterizing surface water with field portable diffuse reflectance spectroscopy, *J. Hydrol.*, *391*, 133–140, doi:10.1016/j.jhydrol.2010.07.014.